WORCESTER POLYTECHNIC INSTITUTE

WPI

Changes in mitochondrial fitness of fibroblasts due to oxidative stress

---

A Major Qualifying Project Report Submitted to the Faculty of

WORCESTER POLYTECHNIC INSTITUTE

in partial fulfillment of the requirements for the Degree of Bachelor of Science

Submitted by:

Sunny Sang Nguyen, BBT

Submitted on:

January 28, 2016

Report Submitted to:

Professor Tanja Dominko, Faculty Advisor, BBT

Abstract

A large contributor to cellular aging is the decline in mitochondrial fitness. The mitochondrial oxidative phosphorylation pathway is responsible for producing adenosine triphosphate (ATP) and reactive oxygen species (ROS) within eukaryotic cells. Using NIH/3T3 mouse embryonic fibroblasts and H_2O_2 as a model of oxidative stress senescence-induced aging, it was found low levels of oxidative stress mimicked senesced traits, weakened mitochondrial and cellular membranes, and decreased levels of cellular ROS and ATP. By understanding the consequences of oxidative stress on mitochondria, insight may be gained for future studies and developments towards a reliable model of aging using more than H_2O_2 as oxidative stressors to replicate cellular aging, as more experimentation is needed.

Acknowledgements

I would like to thank the following people for their time and efforts in helping to complete this project.

- My advisor, Prof. Tanja Dominko, for her professional feedback on this report, presentations, continued guidance and support.
- Dr. Tanja Bele, for her constant assistance in lab, support, and contribution of significant information concerning this project.
- The Biomedical Sciences and Engineering Center at the University of Nova Gorica, for the use of its facilities and equipment, and the faculty, for their support and hospitality.

Table of Contents

Table of Figures

Table of Tables

Introduction

Over the past few decades, medical care standards have improved drastically leading to an increase in global life expectancy. Even so, lifespan varies between individuals as aging is complex and can be defined as a time-dependent decline in functional ability and stress resistance causing physiological and psychological change as well as an increased risk to major geriatric-targeting diseases such as dementia and osteoporosis (Simm et al., 2008; López-Otín et al., 2013). For every individual there is a chronological age and a biological age. Where most individuals can be of the same chronological age, their biological age can differ depending on their environment and upbringing. This biological age or "real" age is poorly defined generating the urgent need of developing biomarkers specific to aging due to their potential impact in diagnostic medicine. The American Federation for Aging Research submitted the following characteristics when developing a biomarker of aging (as reviewed by Simm et al., 2008; and Bürkle et al., 2015):

1. It must predict the rate of ageing. It would tell exactly where a person is in their total lifespan. It must be a better predictor of lifespan than chronological age.
2. It must monitor a basic process that underlies the ageing process, and not the effects of disease.
3. It must be able to be tested repeatedly without harming the individual, such as, a blood test or imaging technique.
4. It must be something that works in humans and in laboratory animals for validation purposes.

One of the consequences of cellular aging manifests itself in reduced mitochondrial fitness. Cellular energy is abundantly derived from the oxidative phosphorylation pathway (OXPHOS) located in the mitochondria. There, the mitochondria produces cellular energy in the form of adenosine triphosphate (ATP) all the while producing by-products in the form of superoxide and hydrogen peroxide grouped together as reactive oxygen species (ROS). The mitochondria lacks repair mechanisms associated with nuclear DNA (nDNA) and so are highly susceptible to oxidative damage resulted from an accumulation of ROS in the mitochondria. This can lead to damage and mutations of the mitochondrial genome (mtDNA) leading towards mitochondrial dysfunction to eventual cell senescence.

I investigated the role of cellular senescence and subsequent aging on mitochondrial DNA through its ATP and ROS formulation, membrane permeability, mitochondrial gene expression, and morphology evident of aging due to oxidative stress.

Background

Mitochondria and the Oxidative Phosphorylation Pathway

Known as the "power plants" of eukaryotic cells, mitochondria are widely populated organelles responsible for generating 90 percent of energy required by cellular molecular systems. Found in the cytoplasm, they obtain the ability to independently divide by simple fission within the cell and contain their own unique mitochondrial DNA (mtDNA) backbone much like bacteria. Surrounded by a double membrane (Figure 1), researchers have theorized this as evidence of an ancient endosymbiotic relationship between a nucleated cell engulfing an aerobic prokaryote brought on by the rising oxygenated environment eventually forming a mitochondrion.

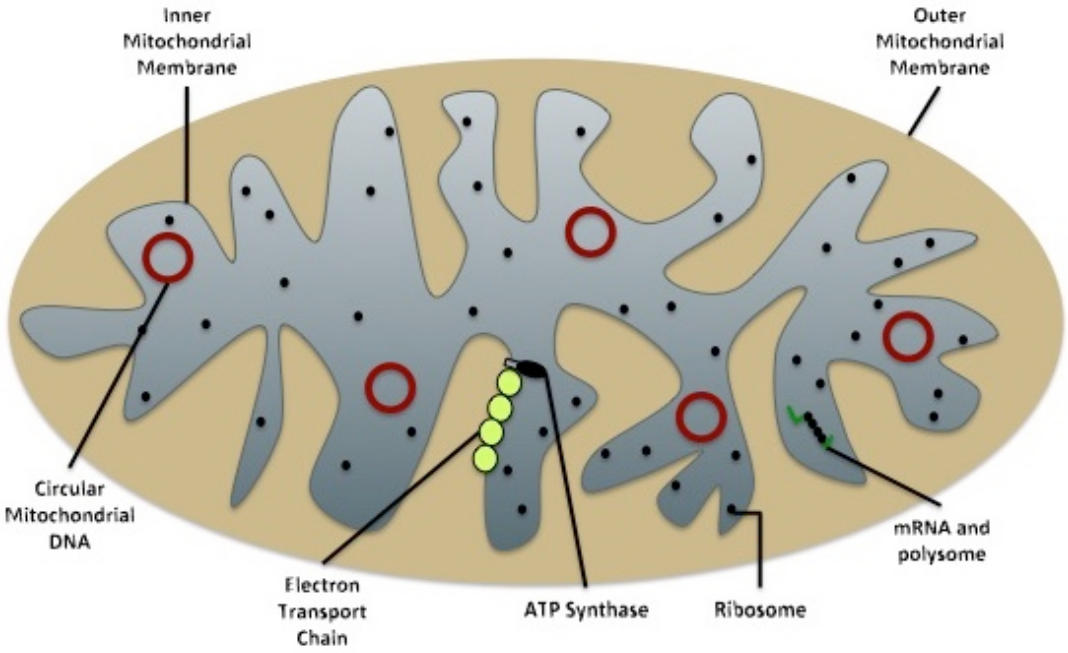

Figure 1. Structure of a mitochondrion (adapted from Lodish et al., 2000).

Mitochondrial DNA (mtDNA) is circular and double-stranded, which supported the evolutionary theory of mitochondria. Surrounded in the inner mitochondrial membrane (IMM) matrix, human mtDNA contains 37 genes coding for two rRNAs, 22 tRNAs required for mitochondrial protein synthesis, and 13 polypeptides (Figure 2) that make up enzymatic complexes featured in the electron transport chain (ETC) and oxidative phosphorylation system (OXPHOS) (Taanman, 1999). Both mtDNA and nuclear DNA (nDNA) contain genes that are responsible for the upkeep of these mechanisms.

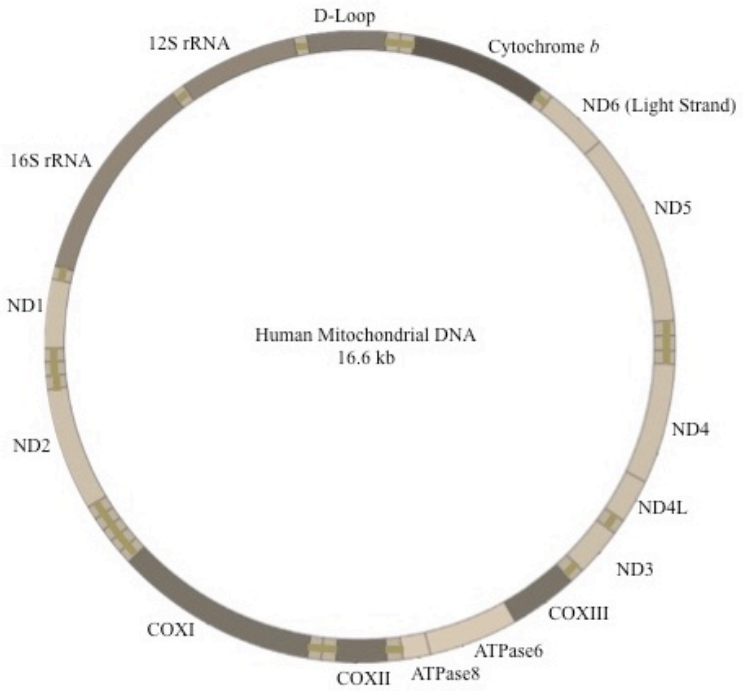

Figure 2. Human mitochondrial genome map.
It contains 37 genes coding for two rRNAs (12S and 16S), 22 tRNAs (unlabeled striped), and 13 polypeptides (labeled). Both the outer heavy-strand and the inner light-strand are represented (adapted from Maechler and Wollheim, 2001).

Often used synonymously, the ETC and OXPHOS are responsible for providing cellular energy in the form of adenosine triphosphate (ATP). The ETC is an aerobic respiratory mechanism found in the IMM, which uses the product of glycolysis, pyruvate, that further oxidizes in the tricarboxylic acid cycle (TCA) cycle (Figure 3). The TCA cycle then provides energy in reduced coenzymes such as nicotinamide adenine dinucleotide (NADH) and succinate that is transferred through the ETC protein complexes eventually converting adenosine diphosphate (ADP) into usable energy, ATP (Lodish et al., 2000).

Complex I, also named NADH-coenzyme Q oxidoreductase, bind with NADH and through redox reactions helps solidify coenzyme Q10 responsible for transferring electrons and proteins released from coenzyme NADH. NADH releases the H^+ proton, which is pumped into the intermembrane space, and the remaining electrons are transported to the next complex in the ETC. A similar process involving succinate to fumarate ($FADH_2$ to FAD) in Complex II also named succinate-Q oxidoreductase (Cooper, 2000) follows this process.

Complex III, known as Q-cytochrome c oxidoreductase, is responsible for the oxidation of ubiquinol and the reduction of cytochrome-c resulting in approximately four H^+ protons which are pumped into the intermembrane space (IMS). What remains is Complex IV, named Cytochrome c oxidase, which is the final complex of the ETC and is responsible for transferring the electrons of the chain to an oxygen molecule (O_2) to form a water molecule (H_2O). This is where OXPHOS comes in with Complex V known popularly as ATP synthase. Protein

complexes I through IV of the ETC uses the resulting differential electrical charge to establish an electrochemical gradient providing energy that drives ATP synthase in complex V of the OXPHOS completing the phosphorylation of ADP to ATP (Figure 3) (Lodish et al., 2000; Cooper, 2000).

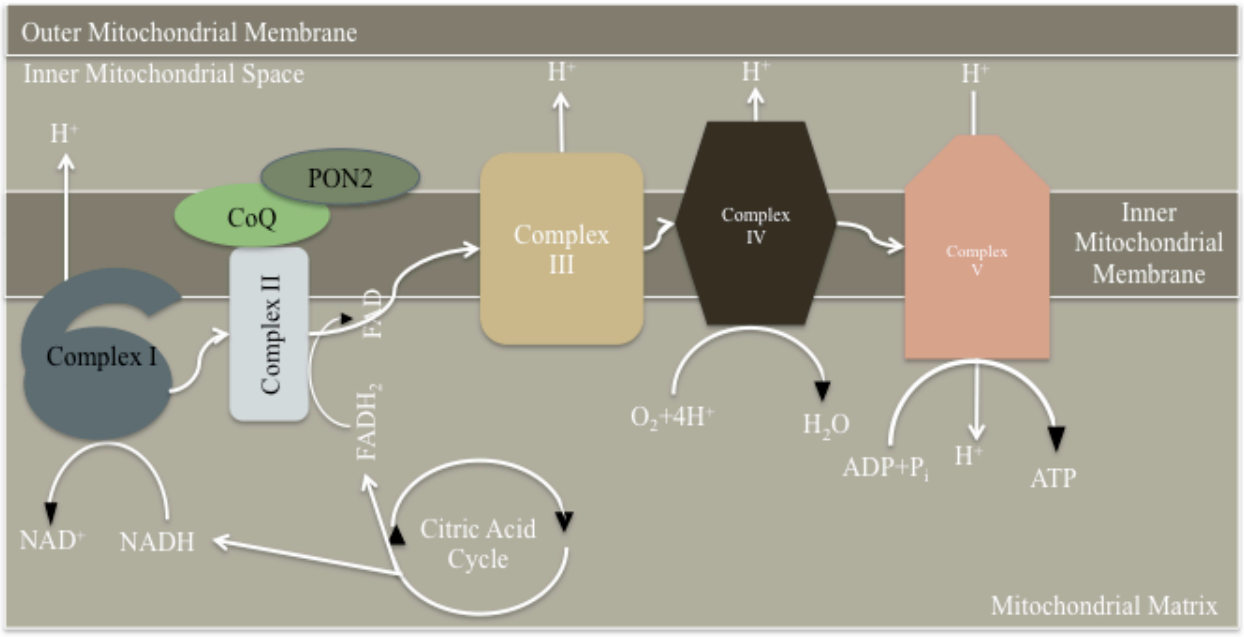

Figure 3. Close up of the ETC (Complex I through IV) and OXPHOS (Complex V) in the mitochondria (adapted from Brownlee, 2001).
Complex I=NADH dehydrogenase complex; Complex II=Cytochrome b-c complex; Complex III=Cytochrome c; Complex IV=Cytochrome oxidase complex; Complex V=ATP synthase; TCA Cycle=Citric acid cycle responsible for generating energy through the oxidation of acetyl-CoA; CoQ=Coenzyme Q10 is needed for basic cell function that helps convert food into energy; PON2=Paraoxonase 2, a D1-like receptor that inhibits ROS production.

ATP is a nucleotide that provides energy for most of the cell activities. It is from the hydrolysis of the third phosphate group of ATP in which a substantial amount of free energy is released. ATPases are responsible for this hydrolysis along with their transport. Because the mitochondrion contains its own genome and replicates independently from the rest of the cell, it makes it easier for mitochondria to multiply when the energy needs of a cell increase. This provides reason for varying populations of mitochondria in differing cell types. It was observed that in the compared findings of thin longitudinal muscle strips between species of goats and dogs, dogs were found to have a greater quantity of mitochondria (Vock et al., 1996). It was concluded that the more aerobic-dependent the cell type (muscle cells) as well as species, the quantity of mitochondria was proportional to maximal aerobic capacity of the cell allowing larger intracellular stores of glucose for energy production. Additionally, mitochondria-rich cell types are found in brown fat tissue, which holds the responsibility for generating heat. Unlike adult humans, infants have mainly brown fat in order to maintain consistent body temperature vital to their survival. In these cell types, much of the mitochondria contain an inner-membrane

protein called thermogenin that functions as an uncoupler of OXPHOS allowing energy conversion of NADH oxidation to heat (Lodish et al., 2000). It was hypothesized that for some aged individuals, the need for overall cellular energy decreases as lifestyles become less active and associated with slower movements and cognitive abilities.

Mitochondrial DNA mutations and their role in aging

Mutations and deletions in mtDNA have been found to contribute to aging and be a frequent cause of genetic disease. Mitochondrial DNA lacks the protective histones and repair mechanisms. Furthermore, because of easy accessibility to completely sequenced human, mouse, and bovine mitochondrial genomes and its common use in both forensic medicine and evolutionary genetic research, studies on mtDNA reveal that though important, altered mtDNA continues to be a focus in understanding their total implications on human health (Taylor and Turnbull, 2005).

In aged human muscle fibers, an increase in segmental, clonal intracellular expansions of unique somatically based mtDNA deletion mutations were found. Mutations in muscle fibers affecting more than 90% of the mitochondrial genome recorded additional loss in cytochrome c oxidase (Complex IV) activity and gain in succinate dehydrogenase (Complex II) activity. Mutations also affected cellular morphology such as fiber splitting, atrophy, and breakage along with electron transport system (ETS) irregularities (Herbst et al., 2006). Additionally, over time mtDNA deletion mutations accumulate in multiple tissues in numerous individuals. When young and aged muscle fibers were compared, the abundance of mtDNA deletion mutations was found inversely proportional to the number of cells analyzed (Taylor and Turnbull, 2005; Herbst et al., 2006; Bua et al., 2006). In addition, in situ hybridization studies denoted the heterogeneous nature of mtDNA deletion mutations throughout a tissue and amplification were localized within certain groups of individual cells. For example, in muscle fibers, mtDNA deletion mutations demonstrated segmental pattern along the fiber length and a mosaic distribution between cells (Herbst et al., 2006; Lopez et al., 2000).

Hundreds of mitochondria, each with its own genome, help create a heteroplasmic environment within the cell. Therefore, it is essential to determine which mutations and consequently gene expression levels are affected by cellular aging. As tissues differ in mitochondrial content, I focused on mouse fibroblasts. It was hypothesized that mitochondrial genome encoded ND1 and ND5 enzymes, both essential to OXPHOS, varied in expression with increased oxidative damage.

Mitochondrial oxidative stress and its role in aging

A widely accepted concept of aging based on Harman's "free-radical theory," the rate-of-living hypothesis, and the role of mitochondria as an energy factory states that as cells produce ATP and the metabolic rate increases, mitochondria generate endogenously generated reactive oxygen species (ROS) that result in mitochondrial damage and mutations compromising energy levels and cellular lifespan (Harman, 1956; Holbrook, 2000). This was evident with the discovery of superoxide dismutase (SOD), an enzyme responsible for the conversion of harmful superoxide

anions to hydrogen peroxide (H_2O_2) produced during normal aerobic metabolism and inflammatory reactions. It was observed that the lifespan of a mutant *Caenorhabditis elegans* lacking SOD any additional ROS superoxide was fatal (Van Raamsdonk & Hekimi, 2012). In human fibroblasts increased SOD expression correlated with a lengthened lifespan under normoxic and hyperoxic conditions (Serra et al., 2013).

In mammalian cells, mitochondria are the major source of ROS. ROS are involved in a number of malignant diseases, including type II diabetes, atherosclerosis, chronic inflammatory processes, and several neurodegenerative diseases (Orrenius et al., 2007). Though generated ROS are a by-product of the ETC, they are not just harmful but play a regulatory role in cellular metabolic process through activation of various enzymatic processes and transcriptional factors. Below a certain threshold of ROS accumulation, ROS acts as a signaling molecule competent enough to induce survival signals to restore cellular homeostasis. Though once passed, cellular senescence signaling is induced (López-Otín et al., 2013).

Approximately 1%-2% of oxygen consumed by the mitochondria is converted into superoxide anions (O2-) by the initial redox reactions in the ETC, which are capable of additional reactions to form ROS including peroxides such as hydrogen peroxide (H_2O_2), aldehydes, and hydroxyl radicals (·OH) (Apel & Hirt, 2004; Liochev, 2013). When ROS accumulation exceeds the detoxifying ability of the mitochondria and cell, the resulting oxidative stress can induce damage on the mitochondria in ways like increased mtDNA mutations, further destabilization of the ETC complexes as in Complex II and IV, or defective quality control by mitophagy, and even cause senescence or eventual apoptosis. A consequence of ROS accumulation is the activation of the mitochondrial permeability transition pore (mPTP). Composed of the IMM adenine nucleotide translocator and the OMM Bax, Bcl2, and cyclophilin D proteins, the activation of the mPTP creates an open channel across the IMM and OMM. This allows for the free diffusion of molecules (< 1,500 Da) between the mitochondrial matrix and the cytosol kicking off the collapse of the transmembrane electrochemical gradient ($\Delta\Psi$), the loss of matrix solutes, and the swelling of the mitochondria (Kokoszka et al., 2001). As a result, proteins such as cytochrome c, procaspases 2, 3, and 9, apoptosis-initiating factors, and caspase-activated DNase are released inducing cytosolic protein and chromatin degradation leading to eventual cell death (Kokoszka et al., 2001). Additionally, mPTP can be activated by not only oxidative stress but also by decreased mitochondrial $\Delta\Psi$, reduced levels of ADP and ATP in the matrix, as well as the uptake of excessive calcium ions (Figure 4). It was hypothesized that as aging occurs, mitochondria specific $\Delta\Psi$ is affected and weakens membrane stability allowing for more leakage of these apoptotic-initiating and cellular senescence-inducing proteins into the cytosol.

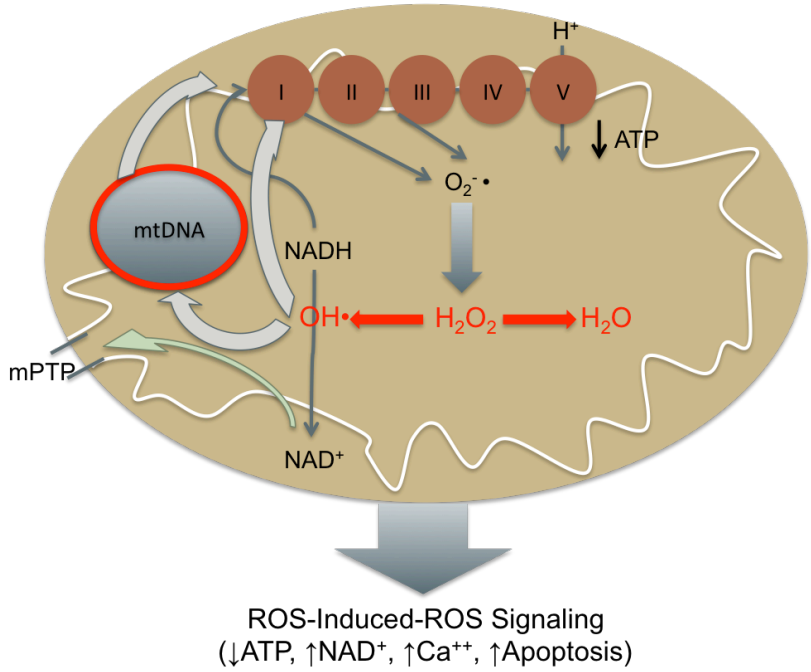

Figure 4. Activation of the mitochondrial membrane permeable transitioning pore (mPTP) by oxidative stress, decreased mitochondrial ΔΨ, reduced levels of ADP and ATP in the matrix, and the uptake of excessive calcium ions.
This can lead to an increase of apoptotic signaling in the cytosol increasing chance of apoptosis (adapted from Dai et al., 2014). I=Complex I; II=Complex II; III=Complex III; IV=Complex IV; V=Complex V; dark orange represents the electron transport chain and the oxidative phosphorylation pathway embedded in the inner mitochondrial membrane.

Mitochondrial oxidative stress has been found to affect aging in mice with targeted mutations of the p66She adapter protein gene displaying reduced ROS generation and increased resistance to ROS-mediated apoptosis and consequently prolonged lifespan (Dai et al., 2014; Dröge and Schipper, 2007). Further studies have shown that this gene is a mitochondrial redox enzyme located in the IMM responsible for producing H_2O_2 during OXPHOS. It was also shown to accumulate in the mitochondrial matrix where it activates mitochondrial calcium ion responses as an apoptosis-inducing factor. Further evidence of aging caused by oxidative stress showed how mice susceptible to mtDNA point mutation and deletion accumulation with age displayed common phenotypes of old age which correlated to their shortened lifespan (Trifunovic et al., 2004). Moreover, mitochondrial oxidative stress has been found to have a central role in mitochondrial pro-apoptotic Bak expression in primary cochlear cells. Mice that had a deletion of the Bak gene were observed to decrease in age-related apoptotic cell deaths of the inner ear cochlea and thus prevented presbycusis (Someya et al., 2009).

Model cellular systems for aging research

Typically, research concerning aging uses promoters of oxidative stress such as ultraviolet radiation (UV) or hydrogen peroxide (H_2O_2) treatments as "accelerants" of aging rather than naturally waiting for the physiological and phenotypical changes often associated with aging. For

example, H_2O_2 in high (≥ 50 μM) concentrations are cytotoxic to cells in culture though this H_2O_2 sensitivity is extremely dependent on cell type and culture conditions used. Whereas, low cultures of H_2O_2 concentrations have been involved in many studies investigating the role of cellular senescence and are the most commonly used inducer for stress-induced premature senescence (SIPS) (Duan et al., 2005). It is even used in studies involving inflammation (de Oliveira-Marques et al., 2007), physiological signaling (Bretón-Romero and Lamas, 2014), and ability to control apoptosis (Li et al., 2009). In Chen and Ames (1994) study, human diploid fibroblast F65 cells were induced into senescence-like states. They found that an average concentration of 200 μM of H_2O_2 was enough to lead to irreversible cellular senescence supported by cells exhibiting senescent-morphological features, irreversible G1 cell cycle arrest, and high senescence-associated ß-galactosidase (SA ß-gal) positivity. With prolonged doses of H_2O_2 treatments on cells (> 1h), induced SIPS resembled replicative senescence at cellular and molecular levels (Duan et al., 2005). Another study found that in MC3T3-E1 and MG63 cells a concentration of 0.5-5 mM of H_2O_2 was needed in order to induce senescence and inhibit mechanistic target of rapamycin (mTOR) signaling (Li et al., 2009). In the NIH/3T3 cell line, different concentrations of H_2O_2 and incubation times can affect whether the cell culture undergoes senescence or apoptosis. Treatments of 100 μM and more promoted cell death which was detected by the staining of viable cells with CellTiter-Blue reagent, but were also incubated for over 16 h (Wang et al., 2007), contrasting to Chen and Ames (1994) findings of 200 μM H_2O_2 treatments over a incubation duration of 2 hours. Furthermore, after a sub lethal dose of H_2O_2 (100-200 μM) treatments between 1-2 h, cells exhibited SIPS along with morphology, growth, and cell cycle arrest similar to that of replicative senescence, SA ß-gal activity, and gene expression (Duan et al., 2005).

Using oxidative stressors like H_2O_2 to induce "aging" is important in *in vitro* cell culture studies. Using H_2O_2 to induce progression of senescence in cells was the most effective model for time-sensitive experiments to investigate mitochondrial characteristics associated with aging. Moreover, as H_2O_2 treatments differ from cell type and culture conditions, it was imperative to investigate the most effective concentration of H_2O_2 necessary in inducing cellular senescence. One cellular system was used in investigating mitochondrial characteristics associated with healthy aging: NIH/3T3 mouse embryonic fibroblasts. It was hypothesized that in aging cellular systems induced by H_2O_2 the ATP and ROS levels would be inversely related. Additionally, gene expression of OXPHOS genes ND1 and ND5 were evaluated after treatments with differing levels of H_2O_2.

Cellular senescence

Cellular senescence is the halt of cell proliferation as a response to apoptotic stimuli, damage, and change of differentiated functions (Figure 5). Cells have a finite replicative lifespan well known as the Hayflick Limit in cell culture. Cell lines differ in their Hayflick Limit, for example mouse embryonic kidney cells (MEK) have a Hayflick Limit of close to 5 replicative passages whereas human embryonic kidney 293 cells (HEK/293) and NIH/3T3 mouse embryonic fibroblast cells, named appropriately after the original desegregated NIH Swiss mouse embryo fibroblasts and the 3T3 culturing protocol meaning "3-day transfer, inoculum 3 x 10^5 cells," can be passaged indefinitely.

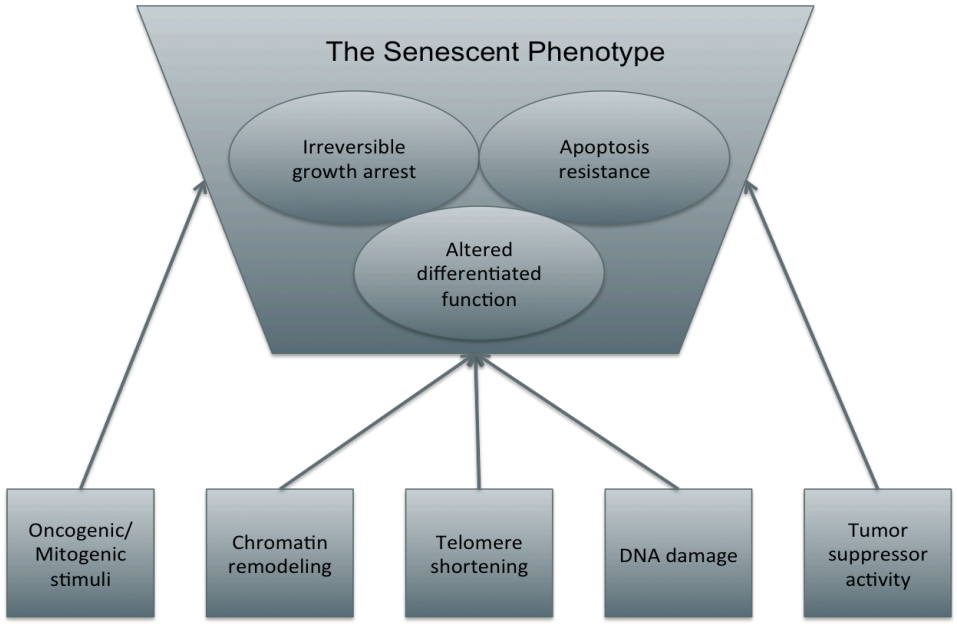

Figure 5. Characteristics and inducers of senescence (adapted from Itahana et al., 2001).

DNA damage is a common characteristic of cellular senescence. Oxidative damage and double strand breaks caused by damage from supraphysiological oxygen concentrations or other stressful *in vitro* culture conditions are possible features of damage (Itahana et al., 2001). Oncogenic stimuli such as activated RAS or RAF proteins, even overexpression of certain tumor suppressor genes such as p16 cyclin-dependent kinase inhibitor (CDKI) (McConnell et al., 1998) and the p14/ARF regulator of MDM2 responsible for negative regulation of the p53 tumor suppressor (Dimri et al., 2000) are capable of inducing cellular senescence.

Cellular senescence in simple terms is a permanent inhibition of cell proliferation. Senescent cells typically arrest growth with a G1 DNA content and cannot be stimulated to resume in cell growth by external factors. Senescent cells resist apoptotic death as well as exhibit changes in morphology, including cellular enlargement, increased lysosome biogenesis, and high sensitivity to ß-gal staining, and differentiated functions in comparison to normal cells (Itahana et al., 2001). For fibroblasts like the NIH/3T3 cell line, fibroblast senescent cells specifically develop a matrix-degrading phenotype that secretes large amounts of matrix metalloproteinases and inflammatory cytokines.

Cellular senescence is also believed to contribute to aging. As a tumor suppression mechanism capable of causing irreversible growth arrest, senescence may be a pleiotropic trait benefiting younger cells and is rather deleterious in older cells making it popular in aging studies. By inducing cellular senescence, senescent cells can be used as models of aged cells making it ideal in investigating mitochondrial characteristics associated with aging.

Objectives

As the quest for prolonged lifespan continues, understanding how human systems interact and damage with age is important in understanding the key factors important in aging and good health. Additionally, knowing how certain exposures to harmful conditions, stressors and predisposed genetics is equally important in developing possible individualized health plans. In this report, *in vitro* culturing of NIH/3T3 mice fibroblasts were used to investigate mitochondrial characteristics in H_2O_2 induced senescence associated with aging. Cells are equipped with a number of mitochondria meant to provide adequate cellular energy for the many processes and reactions that require them. With age, as damages through oxidative and environmental stressors increase, how in turn are the mitochondria affected? This question was investigated following three hypotheses:

Hypothesis 1: Mitochondrial $\Delta\Psi$ collapses with H_2O_2 treatments indicative of a weakened aging membrane.

Hypothesis 2: ROS levels and ATP levels inversely correlate in aging cells as ROS levels rise and ATP levels fall.

Hypothesis 3: Expression levels of mtDNA ND1 and ND5 decrease in H_2O_2 senesced-induced NIH/3T3 cells when compared with the control and actin.

Methods and Materials

Cell culture

The mouse embryonic fibroblast cell line NIH/3T3 (passages 5-15) was obtained from Sigma-Aldrich. Cells were cultured in filtered Dulbecco's modified Eagle's medium [(DMEM); Sigma] supplemented with 2 mM L-glutamine, 100 µg/ml penicillin, 100 µg/ml streptomycin, and 10% heat-inactivated fetal bovine serum [(FBS); Sigma] and incubated in 37ºC humidified atmosphere with 5% CO_2 in air. Cells were passaged regularly; media was changed every two days; and, cells were allowed to reach ≥ 70% confluence before experimental procedures. For experiments involving immunostaining, cells were plated on sterilized glass coverslips in 6-well (5×10^5 per well) and 12-well (5×10^4 per well) plates approximately two days before experimentation. For experimental assays, cells were plated in 96-well (5×10^3 per well) black polystyrene plates. For reverse transcriptase polymerase chain reaction (RT-PCR), cells were plated on four 35 mm tissue culture plates (1×10^5 per well).

Inducing oxidative stress by hydrogen peroxide

To induce oxidative stress to mimic age-related cellular ROS increase, cells were incubated in culture medium containing 0 µM, 50 µM, 200 µM, and 300 µM hydrogen peroxide [(H_2O_2); Sigma] for 2 h on 70%-80% confluent cells. After incubation, cells were washed with PBS thoroughly to remove remaining H_2O_2 residue and prepped for further experimentation. Treated cells were used the day of treatment only in order to prevent issues of degradation and varying post-incubation times.

The effects of H_2O_2 differ between cell lines making it imperative to undergo preliminary concentration treatment experiments. H_2O_2 working concentrations of 0, 5, 15, 30, 50, 100, 200, and 300 µM H_2O_2 were freshly prepared in pre-warmed culture medium then used on NIH/3T3. Duration of incubation time and post-incubation time were also tested. Incubation time was tested at time (t) = 1 h, 2 h, and 3 h. Post-incubation time was also tested at t = 0 (time after treatment), 24 h, and 48 h. Additionally, cells were washed with PBS after treatments and were fixed with 4% paraformaldehyde [(PFA); Sigma], stained with Hoechst-33342/Phalloidin-488 [(dilution 1:1000); Sigma] immunofluorescent stains, then observed and quantified. Samples were mounted in a semi-permanent preparation for final observation. Results were analyzed with the Olympus Model IX81 fluorescence microscope and analyzed with the program SlideBook Edition 4.2 (Olympus). At 200 nm and 488 nm excitation wavelengths, nuclei and actin were observed, respectively. Up to 250 cells were counted at 40X magnification under each concentration characterizing cellular and nuclear morphology (Table 1). Data collected was averaged and Microsoft Excel was used to graphically represent the best H_2O_2 working concentration and incubation times used to induce senescence in NIH/3T3 (adapted from Chen, 1994; Han et al., 2004).

Table 1. Characterizing cellular and nuclear morphology.

Name	Normal	Autophagic	Necrotic	Apoptotic
Description	Round nuclei, reasonable color, no leakage, showed spindle-shaped form	Accumulation of lysosomes, loss of organelles, slight enlargement, oval nuclei	Cell swelling, damaged organelles (enlargement of organelles), large lysosomes, cell lysis	Cell shrinkage, membrane blebbing, nuclear or cellular fragmentation

Immunofluorescence

To determine overall nuclear and cellular morphology, control cells and cells treated with H_2O_2 were fixed with freshly prepared 4% PFA in PBS for 15 min at room temperature. After thoroughly being washed with PBS, the cells were permeabilized in 0.1% Triton X-100 (Sigma) in PBS for 5 min at 37ºC. The cells were further washed with PBS then incubated with Hoechst-33342/Phalloidin-488 [(dilution 1:1000); Sigma] for 5 min at room temperature. Hoechst-33342 is a cell permeable blue nucleic acid stain that tends to bind to A-T rich regions of DNA. Phalloidin-488 is a high-affinity green filamentous actin (F-actin) probe frequently used to visualize cellular structures rather than using phase or DIC filters. Both can be used on live and fixed cells. Cells grown on a coverslip were mounted on microscopy slides with sufficient anti-fading DAPI solution. Cells in tissue culture dishes were immersed in cold PBS. Until examined under the inverted Olympus Model IX81 fluorescence microscope, samples were stored away from light in 4ºC.

Mitochondrial membrane potential

Mitochondrial membrane potential (MMP; $\Delta\Psi_m$) was analyzed by measurement with 5,5′,6,6′-tetrachloro-1,1′,3,3′-tetraethylbenzimidazolylcarbocyanine iodide (JC-1; Molecular Probes). JC-1 is used to detect change in $\Delta\Psi_m$ due to its potential-dependent accumulative nature in mitochondria. At high $\Delta\Psi_m$ JC-1 dye aggregates can be excited at 488 nm. The emission shifts from green (525 nm) to red (590 nm) when J aggregates form. Cell cultures around 70% confluency were plated in 96-well (5 X 10^3 cells per well) black polystyrene plates two days prior to JC-1 measurement. Around ≥ 80% confluency, cells were treated with H_2O_2, washed with PBS and incubated with 10 µg/ml JC-1 dye for 15 min. Ratios of red and green fluorescence emissions were detected using the PerkinElmer 2030 Multilabel Reader Victor™ X2 with accompanying program Workstation 2030 (PerkinElmer). Additionally, imaging was done for JC-1 stained control and treated cells under the microscope (Olympus Model IX81) at excitation wavelengths of ≥ 488 nm (green) and ≥ 580 nm (red) (adapted from Liu et al., 2007).

Cells stained with 5,5′,6,6′- tetrachloro-1,1′,3,3′-tetraethylbenzimidazolylcarbocyanine iodide [(JC-1); (dilution 1:1000); Molecular Probes] were also incubated in live cells along with Hoechst-33342 for 15 min at 37ºC. The cells were washed with cold PBS and immediately observed under the microscope (Olympus Model IX81) at excitation wavelengths of ≥ 488 nm (green) and ≥ 580 nm (red) to view membrane potential. All immunofluorescent microscopy was viewed on either mounted glass slides or cells in PBS saturated environments.

Using MitoTracker CMXRos [(CMXRos); Molecular Probes] as validation of $\Delta\Psi_m$, cells were treated with a lyophilized product dissolved in high-quality anhydrous dimethylsulfoxide (DMSO) to a stock solution concentration of 1 mM. The MitoTracker stock solution (1 mM) was diluted to the final working concentration (50 nM) in culture medium. Cells were plated onto (5 X 10^3 cells per well) black polystyrene plates two days prior to MitoTracker measurement as well as on glass coverslips for imaging. At around 70%-80% confluency, medium was removed from the wells and prewarmed probe-containing working solution (50 nM) was added. Cells were incubated with CMXRos for 30 min at 37ºC. The 96-well plates were measured at excitation wavelengths of ≥ 488 nm (green) using the PerkinElmer 2030 Multilabel Reader Victor™ X2 with accompanying program Workstation 2030. Additionally, imaging was done for MitoTracker stained control and treated cells under the microscope (Olympus Model IX81) at excitation wavelengths of ≥ 580 nm (red). Images were further analyzed with the program SlideBook Edition 4.2 and the ImageJ software. Imaged cells were fixed with 4% PFA and further stained with Hoechst-33342 and Phalloidin-488 as done in previous staining (Pendergrass et al., 2004).

Intracellular ROS and ATP measurement

Cells were plated onto (5 X 10^3 cells per well) black polystyrene plates two days prior to ROS and ATP assays. Control cells and cells treated with H_2O_2 were used to measure H_2O_2 levels using the ROS-Glo™ H_2O_2 Assay (Promega) according to the manufacturer's instructions. Cells were incubated in H_2O_2 treatments for 1 h then allowed to incubate for another 1 h with added H_2O_2 Substrate Solution (20 µl at 125 µM) (included in the kit). The H_2O_2 Substrate Solution provided reacts with H_2O_2 present in the cell, which generates a luciferin precursor. Afterwards, ROS-Glo™ Detection Solution (100 µl) was added and incubated for 20 min at room temperature. The ROS-Glo™ Detection Solution containing Ultra-Glo™ Recombinant Luciferase and D-Cysteine converts the precursor to luciferin by the D-Cysteine, and the produced luciferin reacts with the Ultra-Glo™ Recombinant Luciferase to create a luminescent signal proportional to the H_2O_2 concentration. The relative luminescence was measured using the PerkinElmer 2030 Multilabel Reader Victor™ X2 with accompanying program Workstation 2030. Each assay was run in triplicates and the standard curve included concentrations from 0 µM to 1000 µM (intervals of 100) of H_2O_2 working solutions incubated and measured using the ROS-Glo™ H_2O_2 Assay kit.

Control cells and cells treated with H_2O_2 were used to measure ATP levels using the ENLITEN® ATP Assay System Bioluminescence Detection Kit (Promega) according to the manufacturer's instructions. Each assay was run in triplicates and the standard curve included diluting 10 µl of ATP Standard (included in the kit) with 90 µl of ddH_2O to generate 1 mM ATP standard. Mixed well, 0, 2, 4, 6, 8, 10 µl of the ATP standard (1 mM) was added to blank wells and the volume was adjusted to 50 µl per well with ATP Assay Buffer (included in the kit) to generate 0, 2, 4, 6, 8, 10 nmol per well of ATP Standard. Fluorescence measurement was done according to the manufacturer’s instructions.

RNA isolation and reverse transcriptase-polymerase chain reaction (RT-PCR)

Total RNA from control and H_2O_2 treated NIH/3T3 cells grown on 10 cm tissue culture plates (~80% confluent) were extracted using the RNeasy™ Plus Universal Mini kit (Qiagen) following the manufacturer's instruction. Cells were scraped off their plates using a sterilized cell scraper in 2 ml of PBS then transferred to a 5 ml Eppendorf tube. After labeling the tubes, one 5 mm sterilized glass bead and QIAzol Lysis Reagent (900 µl) (included in the kit) was immediately added to the tubes and vortexed for 5 min to disrupt and homogenize the cells. The lysates were then carefully pipetted into a new microcentrifuge tube and labeled. The homogenate rested on the benchtop for 5 min at room temperature to promote dissociation of nucleoprotein complexes, after which gDNA Eliminator Solution (100 µl) was added and shaken vigorously for 15 s in order to effectively reduce genomic DNA contamination. Chloroform (180 µl) was added and subsequently shaken vigorously for 15 s then allowed to rest on the benchtop for 2-3 min at room temperature. Cells were centrifuged at 12000 x g for 15 min at 4ºC with the upper, aqueous phase transferred to a new microcentrifuge tube. An equal amount of 70% ethanol was added by pipetting up and down then transferred in intervals of 700 µl to an RNeasy Mini spin column in a 2 ml collection tube and centrifuged at ≥ 8000 x g for 15 s at room temperature. This step was repeated for the remaining sample with flow through being discarded each time. After Buffer RWT (700 µl) was added then Buffer RPE (500 µl) with post addition centrifugation at ≥ 8000 x g (15 s and 2 min, respectively). The RNeasy spin column was placed in a new 1.5 ml collection tube and RNase-free water (30 µl) was added to elute the RNA by centrifuging at ≥ 8000 x g for 1 min and repeated using the same added water for increased RNA concentration. After measuring RNA concentration using the PerkinElmer Lambda 40 Spectrophotometer at A260, complementary DNA (cDNA) was synthesized to stabilize the sample and held at 4°C.

Complementary DNA was synthesized for each sample by combining sample RNA extract (16 µl) and Quanta Biosciences qScript reagents (4 µl) containing optimized concentrations of magnesium chloride ($MgCl_2$), deoxynucleotides (dNTP), recombinant RNase inhibitor protein, qScript reverse transcriptase, random primers, oligo(dT) primer, and stabilizers in individual 0.5 ml Eppendorf tubes. Sample tubes were mixed well then incubated in the Mastercycler® (Eppendorf®) to create reverse transcribed cDNA at 25°C (5 min), 42°C (30 min) the temperature activating reverse transcription, 85°C (5 min) the temperature inactivating reverse transcription, then stored at 4°C until PCR amplification.

Newly reverse transcribed cDNA (5 µl) for each sample was transferred to new 0.2 ml microtubes along with 10 µM target upstream primer (1.5 µl), 10 µM target downstream primer (1.5 µl), ddH_2O (6.5 µl), and GoTaq Master Green Mix (12.5 µl) (Promega). Sample tubes were incubated in the Mastercycler® (Eppendorf®) for PCR cycling, which was done as follows: initial denaturation at 95°C (2 min), followed by denaturation at 95°C (45 s); annealing at primer-specific annealing temperature (59°C) for 45 s; and extension at 72°C (15 s) for 50 cycles. Finally, tubes were incubated at 72°C (5 min) for the final extension temperature and stored at 4°C until use.

Three primers sets (MT-ND1, MT-ND5, and Actin) were used in this experiment. The MT-ND1 primers were 5'-GAT CAG GAC ATC CCG ATG GTG-3' (Forward) and 5'-AGC GAA GGG

TTG TAG TAG CC-3' (Reverse). It had a length of 461 base pairs. The MT-ND5 primers were 5'-TCT TCC CAC TCA TCC TAA CCC T-3' (Forward) and 5'-GGT GTG GTC GGG TCT GTT AT-3' (Reverse). It had a length of 458 base pairs.

Actin was used as the loading control. The actin primers were 5'-TCT GGC ACC ACA CCT TCT ACA A-3' (Forward) and 5'-CTT CTC CTT AAT GTC ACG CAC G-3' (Reverse). Following the same procedure for each sample as the sample cDNA above, actin upstream (3 µl) and downstream (3 µl) primers replaced the target primer additions. A negative control was of the same procedure however no sample cDNA was added in order to detect possible contamination or nonspecific amplification in the reaction. The loading and negative controls were amplified in the same PCR cycling conditions as the target primer samples.

The amplified products were analyzed by electrophoresis (loaded 8-10 µl sample per well) on 2% agarose gels containing ethidium bromide (0.5 µg/ml) (AppliChem) to confirm primer specificity and PCR product size. Primers were synthesized by Integrated DNA Technologies.

Agarose (2 g) (Sigma) dissolved in 1X Tris-Acetate-EDTA (100 ml) was poured into a gel mold with a comb after adding ethidium bromide (5 µl). The molded 2% agarose gel was covered with electrophoresis running buffer (1X Tris-Acetate-EDTA) then loaded with the gel ladder (8-10 µl in a single well), loading and negative controls, and amplified samples. The gel ladder was made by combining DNA 100 base pairs Low Ladder (3 µl) (Sigma), ddH_2O (9.5 µl), and GoTaq Master Green Mix (12.5 µl) in a 0.2 ml microtube. The electrophoresis gel was programmed at 80 V for 2 h or 120 V for 1 h.

Results

Determination of hydrogen peroxide concentrations to induce oxidative stress

Replicative senescence in fibroblasts results in an enlarged cell size (Alili et al., 2014) similar to autophagic and early necrotic cells. To check which level of hydrogen peroxide concentrations led to senescent cell morphology, NIH/3T3 mouse embryonic fibroblasts were stained with Hoechst-33342 and Phalloidin-488. Cellular morphology was observed, imaged, and characterized using features listed in Table 1.

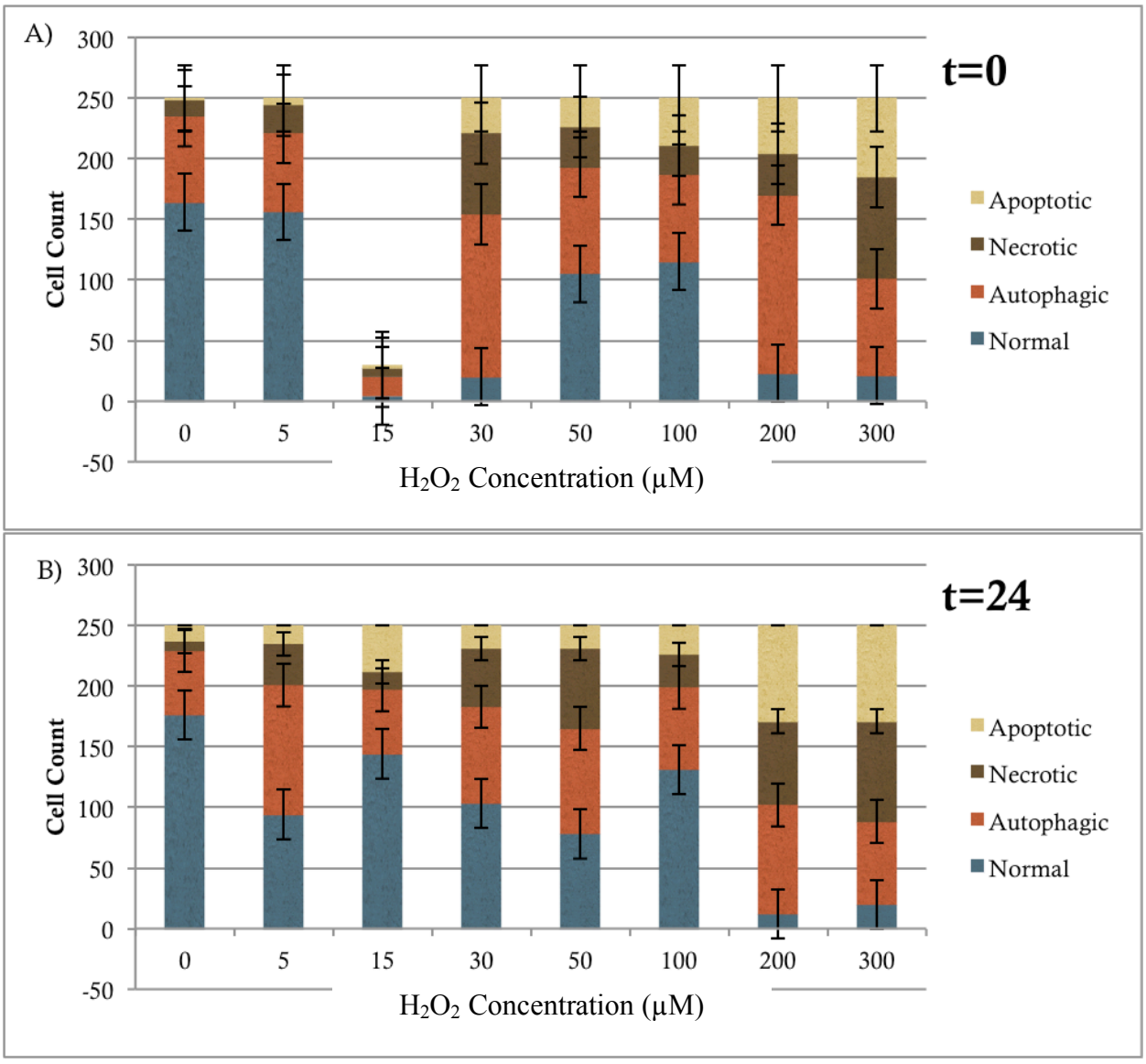

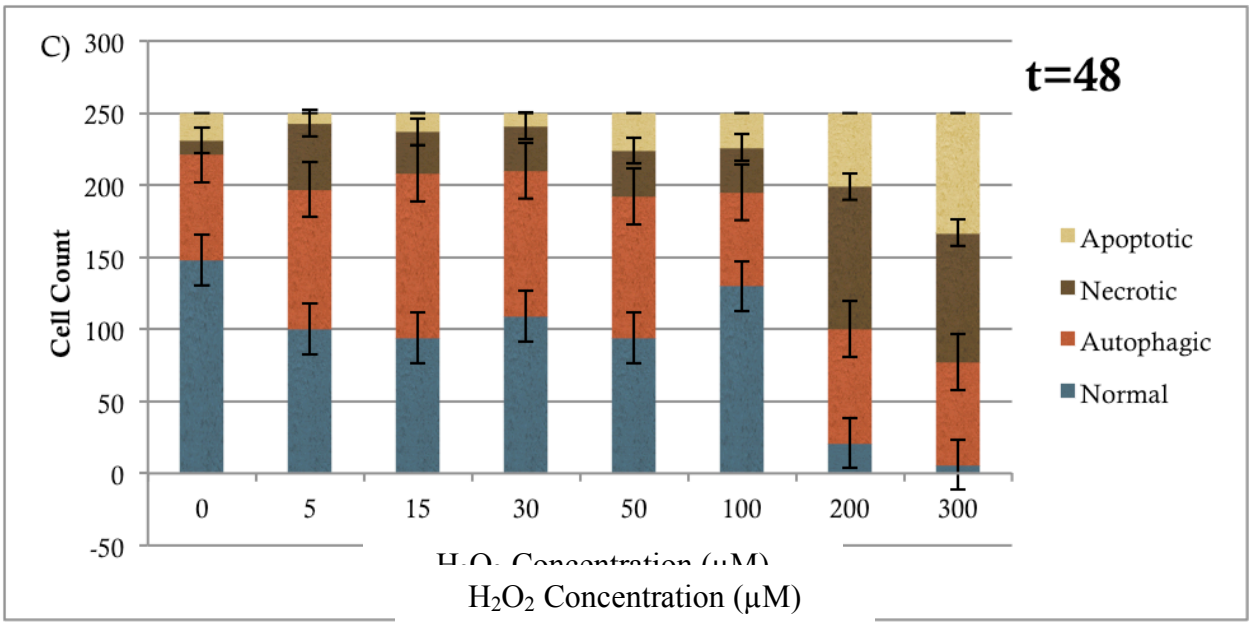

Figure 6. Cytotoxicity and morphology of H2O2 treated NIH/3T3.
NIH/3T3 mouse embryonic fibroblasts incubated with H_2O_2 (5 µM, 15 µM, 30 µM, 50 µM, 100 µM, 200 µM, 300 µM; 2h) at 37ºC and 5% CO_2 in fibroblast growth medium were observed post-incubation over a duration of 72 h. A) By randomization, 25 cells per 10 independent regions per sample were counted for a normalized count of 250 total cells at t=0, 24, 48 h. The experiment was performed as a single independent experiment due to time inconsistency. Standard error is shown. 15 µM data was ignored in t=0 h data due to inconsistency in cell count. B) H_2O_2 treated cells at t=24 h. C) H_2O_2 treated cells at t=48 h.

NIH/3T3 mouse embryonic fibroblasts (passages 5-15) were incubated with H_2O_2 (5 µM, 15 µM, 30 µM, 50 µM, 100 µM, 200 µM, 300 µM; 2h) at 37ºC and 5% CO2 in fibroblast growth medium to determine what concentration of H_2O_2 would be used to induce characteristics of oxidative stress and essentially aging. By randomization, 25 cells per 10 independent regions of one sample were counted for a normalized count of 250 total cells at t=0, 24, 48 h post-incubation with H_2O_2. Figure 6a through 6c reveals the observed morphology of the treated samples. At t=0 h, concentrations ≤ 30 µM H_2O_2 showed high observed cells with normal and autophagic characteristics (Figure 6a). In contrast, high levels of H_2O_2 concentrations showed a slow shift to largely necrotic and apoptotic characteristics. Similar shifts were seen at t=24 h (Figure 6b) and t=48 h (Figure 6c).

To determine the amount of post-incubation time, Figures 6a through 6c were compared individually. Fibroblasts at t=48 h seemed to increase in levels of normal and autophagic morphology after treatment. Focused autophagic and necrotic characteristics were used to determine post-incubation time and concentration amount. At t=0 h, presence of the focus characteristics were greater compared to that at t=24 h. Furthermore, cell counts of autophagic and necrotic characteristics were seen highest between 50 to 200 µM (Figure 6a through 6c). The concentrations 50 µM and 200 µM were chosen due to the inconsistent data presented by 100

μM when compared to the low and high ranges. This may have been due to possible recovery of the fibroblasts (Dai et al., 2014).

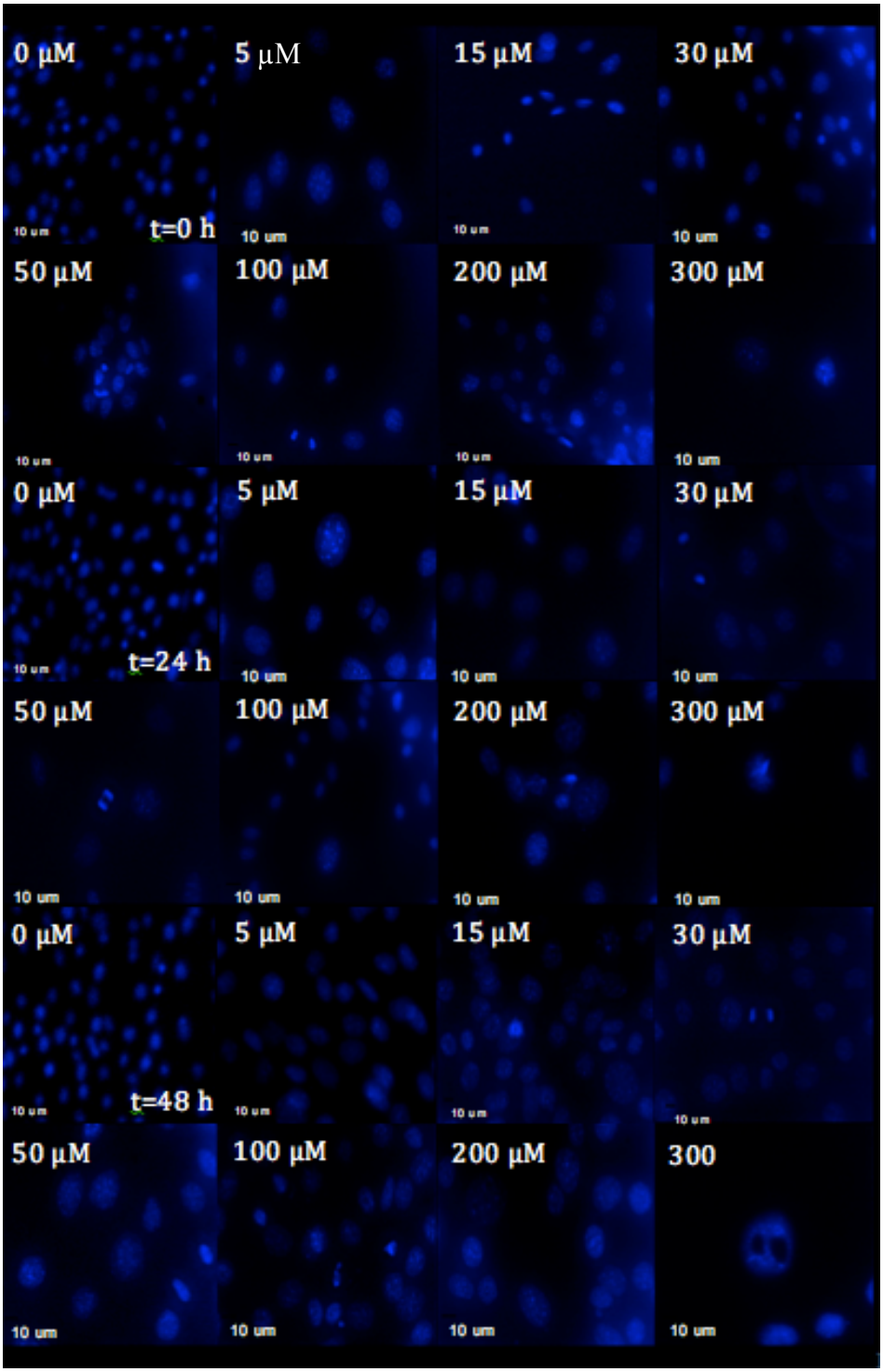

Figure 7. Morphologic changes of cell structure using Hoescht-33342. The experiment was performed as a single independent experiment due to time inconsistency. Magnification scales are shown.

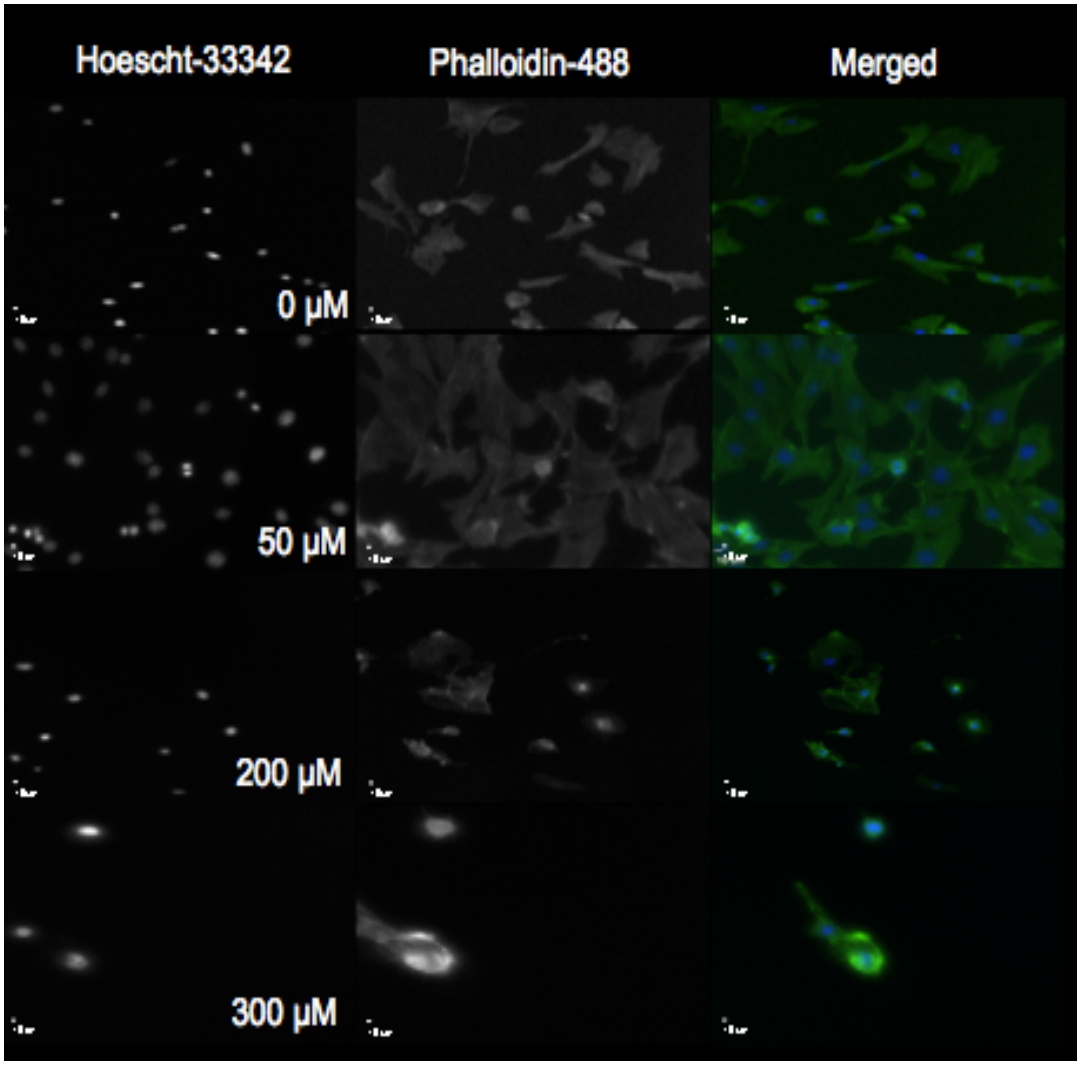

Figure 8. Morphologic changes of cell structure using Hoescht-33342 and Phalloidin-488. The experiment was performed as a single independent experiment due to time inconsistency. Magnification scales are shown.

In Figure 7 and 8, representative images are shown. An increase in cell size was observed until 48 h after treatment with H_2O_2 (Figure 7, t=0 h to t=48 h). Equal incubation with increased post-incubation time provided greater effects on the mitotic characteristics of the fibroblasts. At t=48 h, each H_2O_2 exposed NIH/3T3 sample began to exhibit autophagic and necrotic characteristics. For some in the higher concentrations (200 µM, 300 µM), greater numbers of necrotic and apoptotic morphology were presented. For example, Figure 7, t=48 h, 300 µM shows a fibroblast with an enlarged nucleus and two empty holes showing nuclear damage. Figure 7, t=48 h, 100 µM shows apoptotic blebbing. Figure 7, t=48 h, 50 µM shows enlarged, flat, and oval nuclei indicators of senescent fibroblasts found typically in "differentiated" (aged) fibroblasts (Alili et al., 2014). All cells treated with > 0 µM H_2O_2 showed this morphology. With 5 to 30 µM H_2O_2, this morphology was seen after t=24 h. With 50 to 300 µM H_2O_2, this morphology was seen after t=0. Control (0 µM) fibroblasts had spindle-shaped cell forms with bulges around the nucleus

(Figure 7, 0 μM). This spindle-shape was also seen in early and later post-incubations in 5 to 50 μM (Figure 7, t=0 h to t=48 h, 5 to 50 μM) indicating possible halt in cell cycle.

Additionally, cell numbers present at t=0 h and t=48 h were significantly different. An important marker of replicative senescent fibroblasts is the permanent cell cycle stop not seen in this experiment. Fibroblast count seemed to decrease drastically when compared to the normal at t=0 after treatment in all exposed samples. Whereas, at t=48 h there seemed to be an increase in cell count after treatment indicating that although morphologically there are senescence-induced NIH/3T3, H_2O_2 does not induce permanent senescence and instead produces temporary senescence or transient senescence (Alili et al., 2014).

Concentrations 0 (control), 50, 200, and 300 μM H_2O_2 were tested in a separate experiment with no post-incubation time (t=0) then dyed with Hoescht-33342 and Phalloidin-488 (Figure 8). Spindle-shaped cell forms that are characteristics of mitotic proliferation were observed present in 0 and 50 μM H_2O_2 treated fibroblasts (Figure 8, 0 + 50 μM). At 200 and 300 μM, necrotic and apoptotic cell forms began to overwhelm observations of normal and autophagic morphology. Evidence of degraded or weakened cell membranes was observed in 200 and 300 μM H_2O_2 treated fibroblasts (Figure 8, 200 + 300 μM).

Analysis of mitochondrial membrane potential of H_2O_2 treated NIH/3T3 cells

ROS accumulation becomes more prevalent in aging mitochondria, which can activate the mitochondrial permeability transition pore (mPTP). Found in the IMM, the mPTP creates an open channel across the inner and outer mitochondrial membrane. This free diffusion of molecules (< 1,500 Da) allows the release of harmful proteins capable of inducing cytosolic protein and chromatin degradation leading to apoptosis. To measure whether mitochondria specific $\Delta\Psi$ is affected and weakened due to H_2O_2, a known ROS, mitochondria membrane potential sensitive dye JC-1 and dye CMXRos were used.

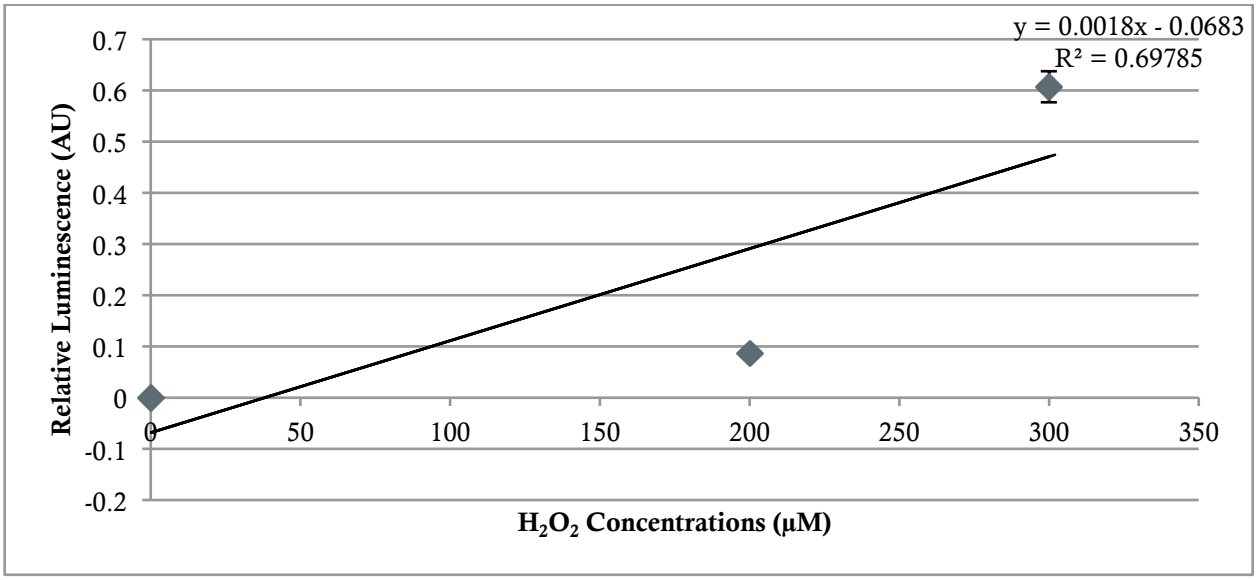

Figure 9. JC-1 membrane potential analysis post H_2O_2 treatments.
NIH/3T3 mouse embryonic fibroblasts (passages 5-15) were incubated with H_2O_2 (50 µM, 200 µM, 300 µM; 2h) at 37ºC and 5% CO_2 in fibroblast growth medium. After, live cells were incubated with 10 µM/ml JC-1 membrane potential dye (Molecular Probes) along with Hoechst-33342 (Sigma) at 37ºC for 15 min. Relative luminescence (RT) of cells were measured at excitation wavelengths of ≥ 488 nm and ≥ 580 nm using the PerkinElmer 2030 Multilabel Reader Victor™ X2. Graph shows normalized ratios using arbitrary units (AU). The experiment was performed as three independent experiments and averaged. Linear equation resulted in y=0.0018x-0.0683 with an R^2-value of 0.69785. Standard error bars are shown for both axes.

JC-1 is a lipophilic cationic probe whose monomer emits a green color (≥ 488 nm) at depolarized membrane potentials that forms aggregates associated with large shifts in emission to red-orange (≥ 588 nm) at hyperpolarized potentials, depending on the mitochondrial membrane potential. Live cells treated with H_2O_2 concentrations (µM) provided two luminescence values at ≥ 488 nm and at ≥ 580 nm. These values were used to estimate the relative red:green (≥ 580 nm:≥ 488 nm) ratios of each concentration. Three independent experiments were performed and averaged (See Appendix B).

JC-1 red:green ratios (Figure 9) were found to increase numerically as H_2O_2 concentrations (µM) increased. The mean values provided a linear equation of y=0.0053x-1.8708 with an R^2-value of 0.11621. The low coefficient of determination was caused by the 50 µM ratio increase. Raw JC-1 data (Figure B1 in Appendix B) reveals that at 50 µM, both averaged values of luminescence at ≥ 488 nm and at ≥ 580 nm were of approximate equal resulting in a value of 1 AU. The increase in red:green ratio may have been influenced by the loading times of the dye since J-aggregates form in a concentration-dependent manner. Furthermore, cells were immediately measured after the 15 min incubation of JC-1. Raw JC-1 measurements (Figure B1 in Appendix B) reveal the increasing difference between red luminescence and green luminescence. There were larger levels of luminescence for the red-fluorescence indicating hyperpolarization in all H2O2

concentrations. JC-1 being a cationic dye tends to accumulate in mitochondria due to their largely negative membrane potential when compared with the rest of the cell. Therefore, the cells may have been influenced by possible plasma membrane hyperpolarization.

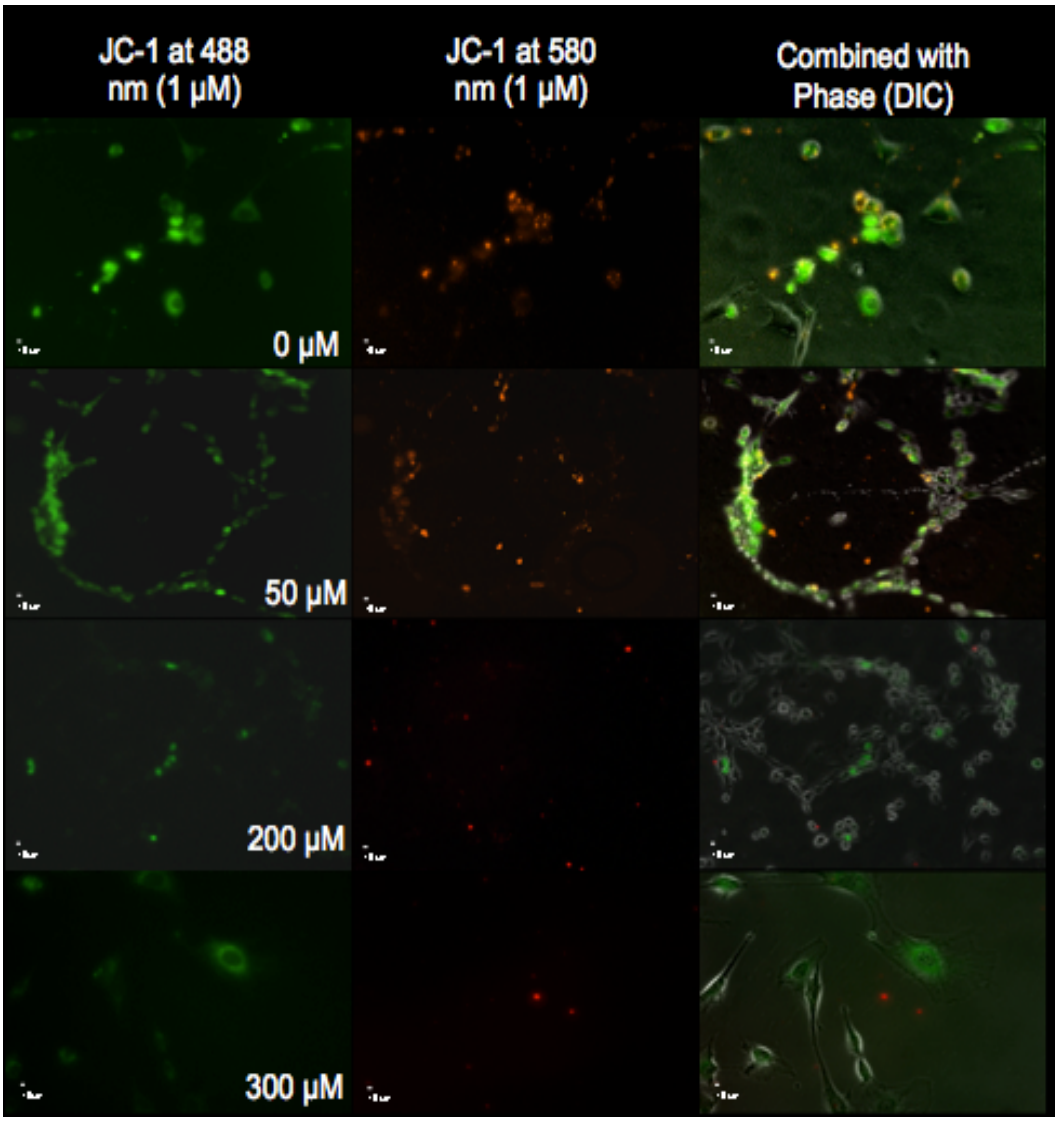

Figure 10. NIH/3T3 fibroblasts post H2O2 treatments dyed with the mitochondria membrane potential sensitive dye JC-1.
Cells dyed with JC-1 were observed at excitation wavelengths of ≥ 488 nm and ≥ 580 nm to view membrane potential. Magnification scales are shown.

Figure 10 reflects images obtained from an independent experiment from that of the measured ratios in Figure 9. Dissimilarly from that of Figure 9, Figure 10 shows decreasing red fluorescence with increasing H_2O_2 concentrations. It also highlights the mortality of the fibroblast due to high exposure of ROS. In the control and 50 µM samples, the red J-aggregates are displayed throughout the individual cells with some clumping. At 200 µM and 300 µM, the J-aggregates are seen less frequently and instead of equal dispersion throughout the cell the red

fluorescence is not located in senesced cells (Figure 10, 300 µM). Present fluorescence may be background interference. Green fluorescence is seen dispersed throughout the cell with localization around the nuclei as seen in by the darker circle form outlined by dyed mitochondria within the cell (Figure 10, 0 µM). The same is seen at 300 µM H_2O_2.

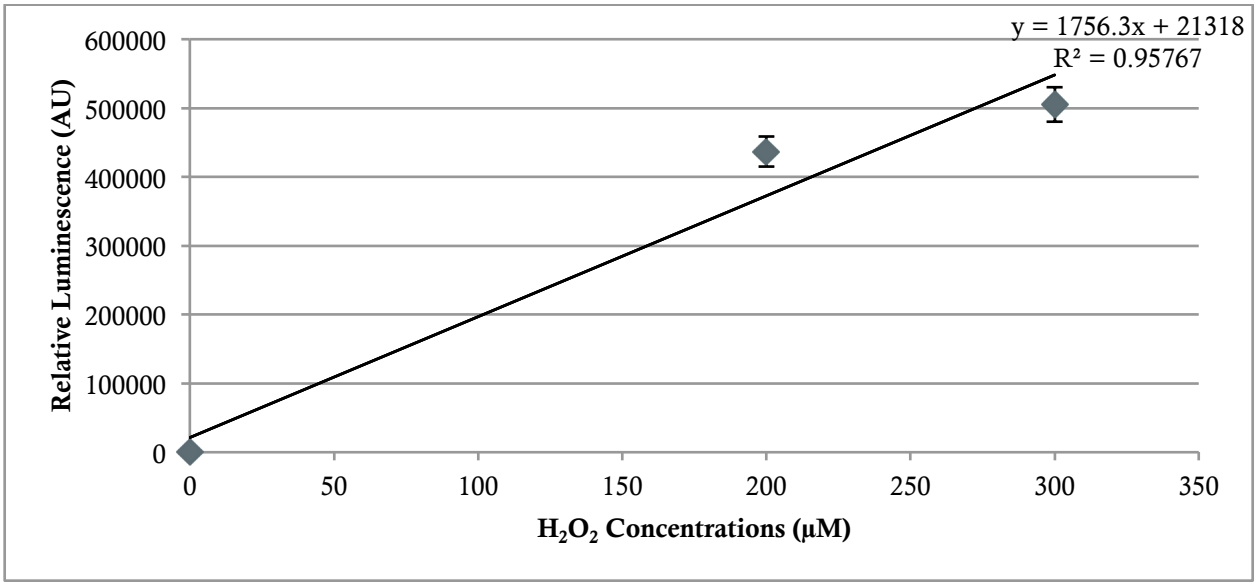

Figure 11. MitoTracker CMXRos analysis post H_2O_2 treatments.
NIH/3T3 mouse embryonic fibroblasts (passages 5-15) were incubated with H_2O_2 (50 µM, 200 µM, 300 µM; 2h) at 37ºC and 5% CO_2 in fibroblast growth medium. After, live cells were incubated with 50 µM CMXRos dye for 30 min at 37ºC then with Hoechst-33342 and Phalloidin-488 (Sigma) at 37ºC for 15 min. Relative luminescence (RT) of cells were measured at excitation wavelengths of ≥ 488 nm and ≥ 580 nm using the PerkinElmer 2030 Multilabel Reader Victor™ X2. Graph shows normalized ratios using arbitrary units (AU). The experiment was performed as three independent experiments and averaged. Linear equation resulted in y=1756.3x+21318 with an R^2-value of 0.95767 omitting 50 µM. Standard error bars are shown for both axes.

MitoTracker Red CMXRos (CMXRos) is a red-fluorescent dye (≥ 488 nm) that stains mitochondria in live cells and its accumulation is dependent upon membrane potential. To analyze the mitochondrial membrane potential ($\Delta\Psi_m$) using CMXRos, NIH/3T3 mouse embryonic fibroblasts (passages 5-15) were incubated with H_2O_2 concentrations for 2 h at 37ºC. then further incubated with CMXRos (50 µM), Hoechst-33342, and Phalloidin-488 for 15 min at 37ºC. Using the PerkinElmer 2030 Multilabel Reader Victor™ X2, the relative luminescence (AU) of CMXRos dyed samples were measured at ≥ 488 nm. Three independent experiments were performed and averaged (See Appendix B).

In Figure 11, the mean values provided an increasing linear equation of y=1756.3x+21318 with an R^2-value of 0.95767. Measuring CMXRos fluorescence, it is important to see an increase in red fluorescence as CMXRos is membrane potential dependent, so as membrane potential

decreases due to a weakened membrane a higher red is found resulting in the increased linear trendline (Figure 11).

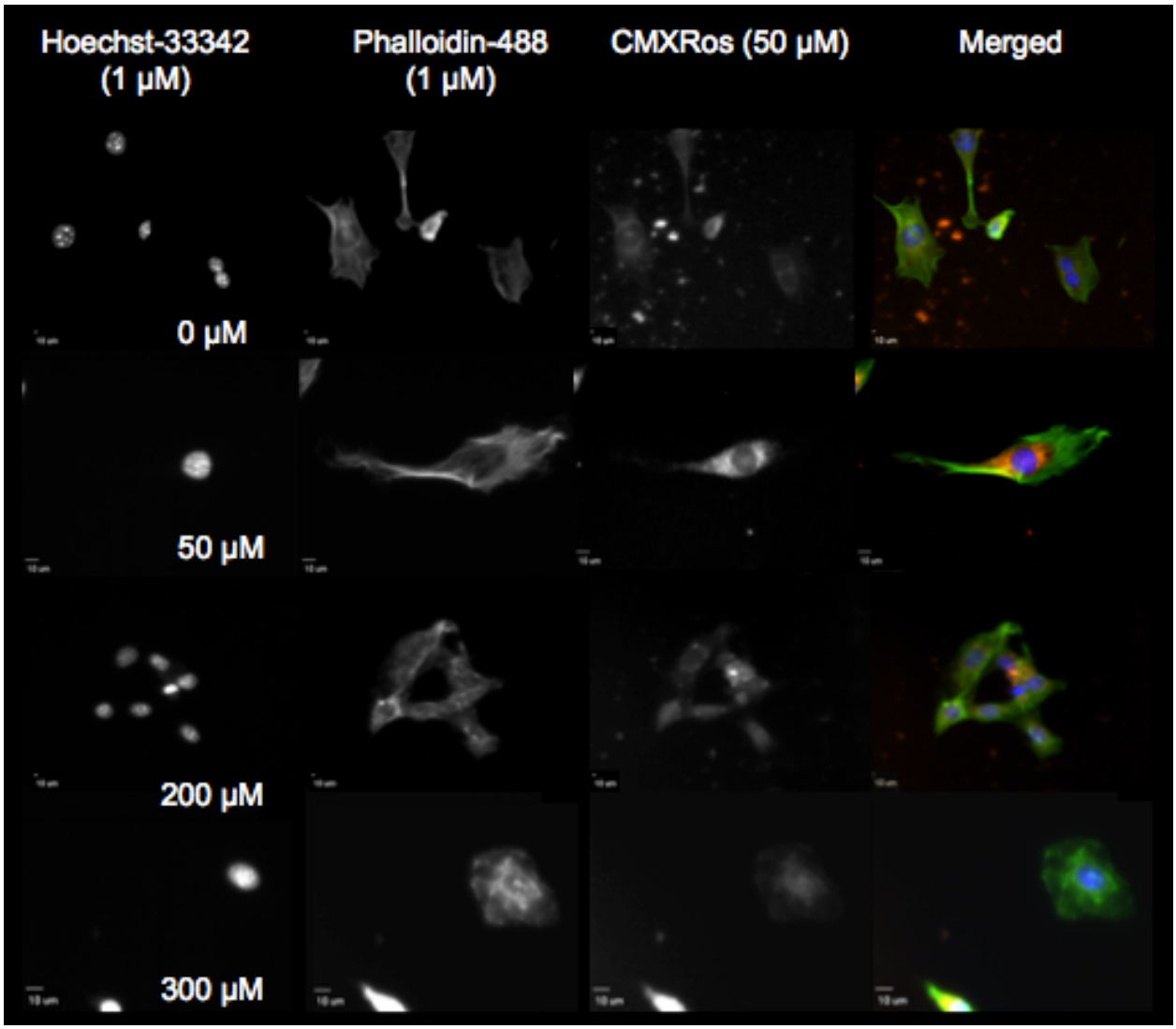

Figure 12. NIH/3T3 fibroblasts post H_2O_2 treatments dyed with MitoTracker CMXRos, Hoescht-33342, Phalloidin-488, and merged.
Cells dyed with CMXRos were observed at excitation wavelengths of ≥ 488 nm and ≥ 580 nm to view membrane potential. Magnification scales shown.

Figure 12 represents images obtained from H_2O_2 treated fibroblasts dyed with CMXRos. Hoechst-33342 and Phalloidin-488 are visuals showing the senescence characteristic induced by oxidative stress such as the enlarged and oval nuclei. The green actin stain Phalloidin-488 shows a lean and long cellular membrane in the control reverting to a more detached and closed-in membrane at 300 µM. Interestingly, CMXRos reveals a decrease in localization (Pendergrass, 2004). The clear nuclei outline formed by the mitochondria presence close to the nuclei

showcases the more important organelles. Rather than clumping, higher concentrations such as 300 µM reveals a less outlined nuclei indicating mitochondria dispersal.

Quantification of intracellular ROS and ATP of H_2O_2 treated NIH/3T3 cells

Mitochondria provide cellular energy in the form of ATP. It is a result of the ETC (Complex I through IV) and OXPHOS (Complex V) at work in the inner mitochondrial membrane (IMM). ROS is a by-product of these two systems; and, a large accumulation of ROS in the IMM can cause damage to mtDNA and IMM proteins resulting in decreased efficiency or signaling of apoptosis. To check whether increased oxidative stress leads to increased ROS levels and decreased ATP levels in the mitochondria, quantification of intracellular ROS and ATP were measured using ROS-Glo™ H_2O_2 Assay Kit (Promega) and ENLITEN® ATP Assay System Bioluminescence Detection Kit (Promega), respectively (Figure 13).

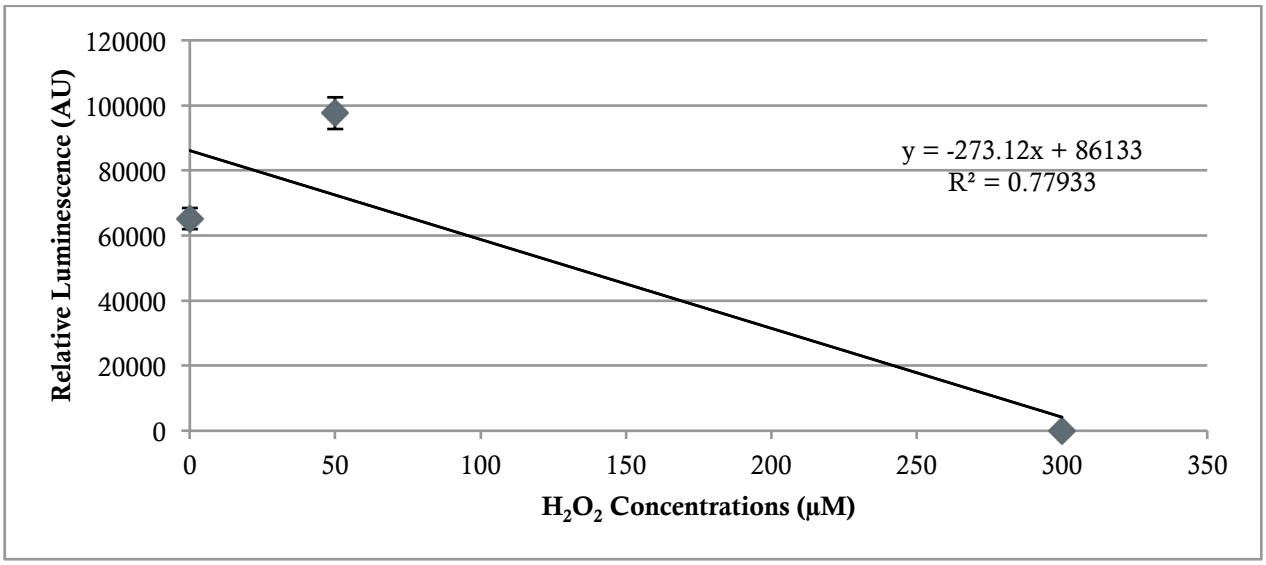

Figure 13. ROS levels after H_2O_2 treatments.
Using the ROS-Glo™ H_2O_2 Assay (Promega) according to the manufacturer's instructions control and treated H_2O_2 cells were used to measure H_2O_2 levels. Relative luminescence was measured using arbitrary units (AU). Linear equation resulted in y=-273.12x+86133 with an R^2-value of 0.77933. Standard error bars are shown.

Using the ROS-Glo™ H_2O_2 Assay (Promega), six independent experiments were performed, averaged, and normalized along with a ROS standard (See Appendix C). Data values were plotted and the linear trendline found was y=273.12x+86133 with an R^2-value of 0.77933. With a coefficient determination of 77.9%, the trendline cannot confidently be characterized accurately as linear. However, the normalized data (Figure 13) reveals a relative decrease in luminescence (AU). ROS levels decreased with the increased H_2O_2 concentrations (µM).

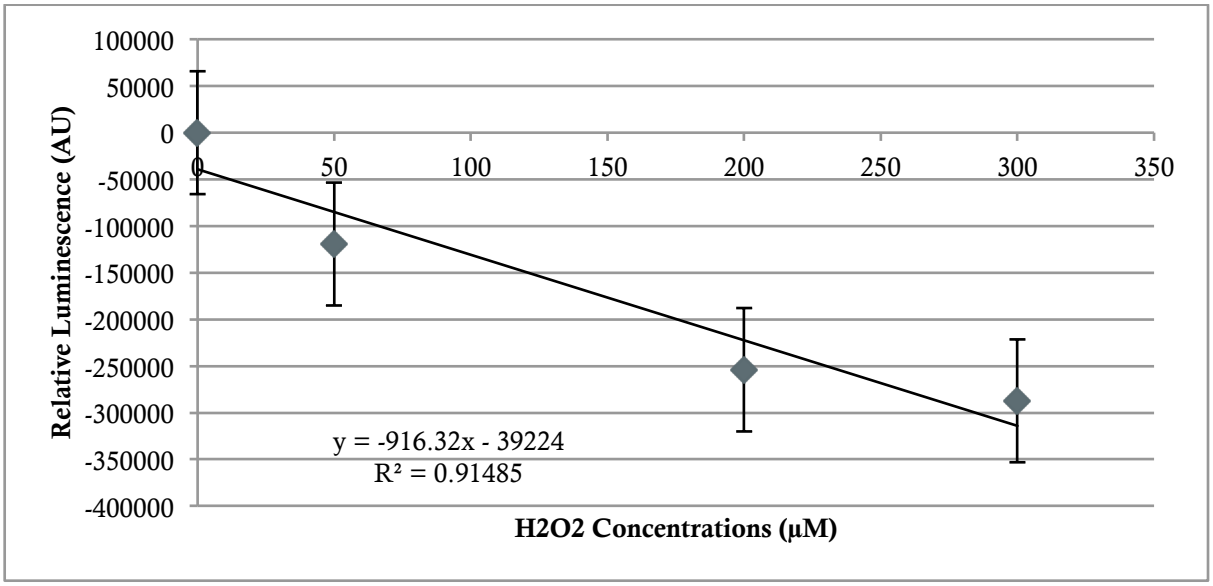

Figure 14. ATP levels after H_2O_2 treatments.
Using the ENLITEN® ATP Assay System Bioluminescence Detection Kit (Promega) levels of ATP were measured according to the manufacturer's instructions. Relative luminescence was measured using arbitrary units (AU). Linear equation resulted in y=-916.32x-39224 with an R^2-value of 0.91485. Standard error bars are shown.

Using the ENLITEN® ATP Assay System Bioluminescence Detection Kit (Promega), six independent experiments were performed, averaged, and normalized along with an ATP standard (See Appendix D). Data values were plotted and the linear trendline was found to be y=-916.32x-39224 with an R^2-value of 0.91485. With a coefficient determination of 91.5%, the trendline is extremely close to the measured data. Normalized data (Figure 14) reveals the relative decrease in luminescence (AU). ATP levels decreased with the increased H_2O_2 concentrations (µM).

MT-ND1 and MT-ND5 mRNA expression in H_2O_2 treated NIH/3T3 cells

Total RNA from control and H_2O_2 treated NIH/3T3 cells grown on 10 cm tissue culture plates (~80% confluent) was extracted using the RNeasy™ Plus Universal Mini kit (Qiagen) following the manufacturer's instruction. Through preliminary investigation, extracted RNA yielded extremely low presence of RNA. However, cDNA was synthesized using the low RNA yields and its concentration was determined by spectrophotometry. RT-PCR was run for MT-ND1, MT-ND5, and actin (load control).

Agarose gel electrophoresis analysis of the RT-PCR with MT-ND1, MT-ND5, and actin (Figure 15) shows non-specific binding for primers MT-ND5 and reveals some unknown bands. The predicted size of MT-ND1, MT-ND5, and actin is 461, 458, and 316 base pairs (bp), respectively.

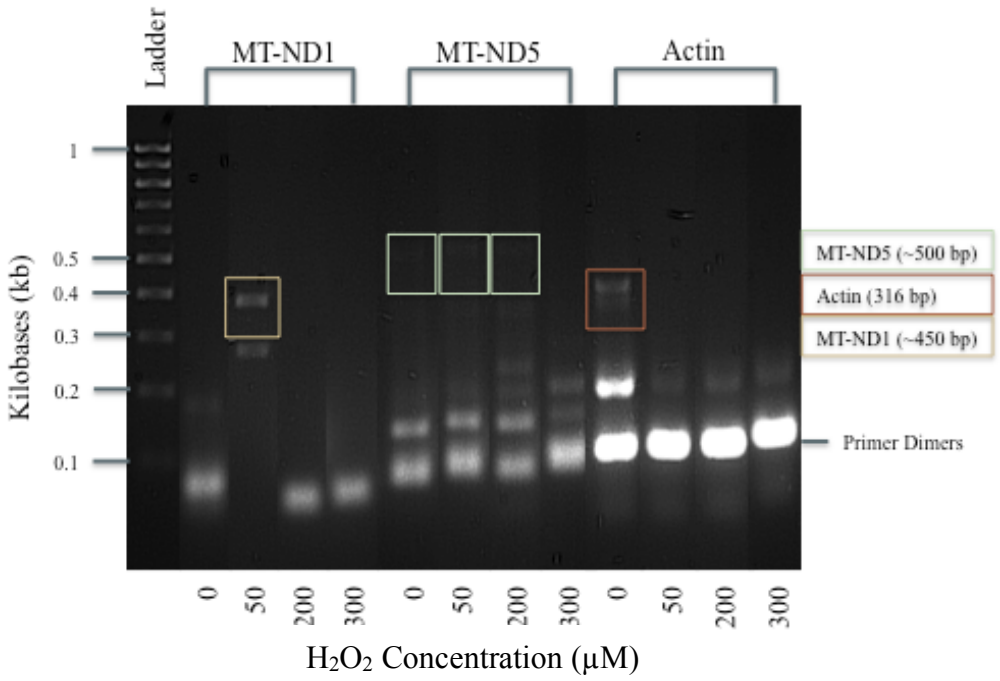

Figure 15. Agarose gel (2%) electrophoresis of RT-PCR target products.
The gel picture shows the presence of primer-dimers in all lanes except 50 µM MT-ND1. MT-ND1 shows possible target RNA (~0.38 kb) at 50 µM and an unknown band at ~0.29 kb. MT-ND5 shows possible target RNA (~0.5 kb) at 0, 50, and 200 µM with varying unknowns around 0.15 kb to 0.2 kb. Actin shows band at 0 µM (~0.5 kb) and no remaining bands for 50, 200, and 300 µM.

Expression levels of actin (loading control) appear to decrease or be non-existent over increasing H_2O_2 concentrations (µM). For each lane, there shows a consistent band (≤ 0.1 kb) aside from MT-ND1 at 50 µM. These are most likely primer dimers, which tend to be between 0.05 kb to 0.1 kb. The slant line is more visually apparent the further right the sample is from the ladder that may be caused by uneven gel thickness or poor flow of electrical current.

Alternatively, the increased bands could be fault of poor primer designs. MT-ND5 shows three faint bands at approximately 500 bp from 0, 50, and 200 µM and a non-existent band at 300 µM. Below that shows four distinct bands at approximately 0.15 kb that decrease in expression with each increase in H_2O_2 treatments (µM). Overall, the gel provided inconclusive results.

Discussion

Aging is associated as a time-dependent decline in physiological and psychological ability. A result of several factors, it is postulated that oxidative stress is a major cause of aging. Oxidative stress is an imbalance between the accumulation of free radicals and the body's neutralization ability. Constant formation of free radicals such as reactive oxidative species (ROS) is the main characteristic of all living systems that use oxygen for their basal metabolism (Abdollahi et al., 2014). An integral part of basic cell regulation and signaling pathways, the most common ROS are superoxide radicals (O_2^-) and hydrogen peroxide (H_2O_2).

Harman's "free-radical theory" of aging considers that as mitochondria produce ATP and the metabolic rate increases, mitochondria generate significant levels of ROS that result in critical damage to macromolecules in the organelle. High ROS accumulation and decrease in antioxidant enzymes equally lead to oxidative stress, enzyme inactivation, and mitochondrial and cellular dysfunction (Abdollahi et al., 2014; Holbrook et al., 2000). Though recently, the free-radical theory has gained new criticism.

Tackling issues such as geriatric and oncologic concerns, increased levels of H_2O_2 have been used to induce replicative senescent fibroblasts (Alili et al., 2014) in order to model aging. Toussaint et al. (2000) show stress-induced premature senescence (SIPS) caused by oxidative stress using H_2O_2. Fibroblasts undergone treatment with varying concentrations of H_2O_2 induced premature senescence in fibroblasts for an overall duration of three days showing characteristics of lack of replicative ability (mitotic spindle), altered cell morphology, and increased levels of ROS. However, the treated fibroblasts induced transient senescence as fourteen days after treatment ROS levels decreased and cells began to replicate. Similar premature senescence was witnessed in fibroblasts treated with H_2O_2 in a study conducted by Duan et al. (2005) and H_2O_2 - induced senescence was maintained over fourteen days only when continuously treated with H_2O_2 (Alili et al., 2014). Studies connecting ROS levels and lifespan are debatable, Perez et al. (2009) showed that as ROS levels decreased the lifespan of mice were neither lengthened nor shortened. There was little effect.

However, ROS are responsible for certain aspects of cellular damage. Examples include mitochondrial membrane (Roberg et al., 1999) and mtDNA damage (Atilano et al., 2009). Using H_2O_2 as an oxidative stress inducer, NIH/3T3 fibroblasts were senescence-induced. Treated fibroblast at concentrations of 50 and 200 μM H_2O_2 largely obtained characteristics of SIPS such as enlarged and oval nuclei, weakened and slightly detached cellular membrane, and proliferation stop (Figure 6).

Treated fibroblast mitochondria $\Delta\Psi$ were observed using fluorescence dyes JC-1 and CMXRos. JC-1 detects change in $\Delta\Psi_m$ by observing shifts in emission from red-orange to green signifying hyperpolarized potentials to depolarized potentials. Figure 9 compared to Figure 10 showed varying results partly due to the poor filters of the multilabel reader. To remedy the inconsistency, optical plates were measured in triplicates, averaged, and normalized. Though a positive linear trendline was formed, images showed the decrease in hyperpolarized potential and remaining depolarized potential in mitochondria. Interestingly at higher levels of H_2O_2

concentrations, mitochondria surround the nuclei as if to increase ATP transmission. CMXRos (Figure 8) exhibits similarities. The trendline formed increases that correlate with increased dye intake of highly depolarized mitochondria (Pendergrass et al., 2004). Furthermore, images display the loss of localization of the mitochondria. As fibroblasts are treated with higher sub toxic concentrations of H_2O_2 mitochondria, instead of surrounding the nuclei to conserve energy assuming for transfer pathways or ATP transport, are highly dispersed across the cell but still remain in the vicinity of the nuclei.

It was also hypothesized that in aging cells ROS levels increase by accumulating in the mitochondria (Dai et al., 2014; Alili et al., 2014), and ATP levels decrease resulting in nuclear damages and structural instability (transport, efficient ion production) caused by ROS. Data revealed that ROS levels actually decreased (Figure 13) contradicting the proposed hypothesis. It is unclear as to why this data occurred, as it is logical to assume an increase would occur as the ROS-Glo™ H_2O_2 Assay measures H_2O_2 specifically. Additionally, ROS (H_2O_2) was used to treat the NIH/3T3 fibroblasts to simulate cellular aging. Instead, the decreasing trendline (Figure 13) indicated that either NIH/3T3 fibroblast have a peak H_2O_2 sensitivity of approximately 50 μM H_2O_2 or that during the incubation process for simulating cellular aging was too long resulting in complete destruction of any cellular body. There may also have been an experimental error in either prepping for ROS measurement, the inaccuracy of the multilabel reader, or the provided ROS measurement kit. In contrast, ATP levels decreased (Figure 14) with high levels of H_2O_2 concentrations supporting part of the proposed hypothesis.

Expression levels of MT-ND1 and MT-ND5, mtDNA genes associated with Complex I of the OXPHOS were measured using RT-PCR (Figure 15). Bands were unclear and extremely weak. This may have been a fault of poor primer design as intense bands at around 0.05 kb were found in almost all samples indicative of primer dimers. Going through primer design, it may have been due to incompatibility issues between the primer and the experimental subject. MT-ND1 and MT-ND5 are accompanying codes for the human mitochondrial DNA whereas the experimental subject used throughout this report was that of an NIH/3T3 mouse embryonic fibroblast. Seeing as those two are of completely different species, that may have been one of the key reasons for low RNA extraction, low DNA content, and poor unidentifiable agarose gels. If forgoing that information, the information the gel does reveal is a band at 50 μM for MT-ND1 but not at the control. MT-ND5 revealed three faint bands at approximately 500 bp from 0, 50, and 200 μM and a non-existent band at 300 μM. Below those bands revealed four distinct bands at approximately 0.15 kb that decrease in expression. Both could be indicators of decreased expression due to oxidative stress. Unfortunately, a single set of samples was used with no accompanying positive or negative controls, rather than running triplicates, leading to inconclusive data.

Understanding the consequences of oxidative stress on mitochondria is essential in studies concerning future aging and mitochondrial disease. From subsequent studies and the data herein, ROS is not alone in inducing senescence and does not accurately depict aging. It is imperative to understand how in aging do cells replenish keeping out bodies healthy and strong with proper healthcare and continue to proliferate. It is also imperative to understand which characteristics such as which string of proteins are indicators or even responsible for aging. This is where more

research should be done to fully understand in a systematic approach to how cells age. As we age, cells do not simply die, they continue replicating until cell death. At what stage does the repair mechanisms of cells weaken so much that not only tissue is affected but also the overall organ and body are affected? Environmental toxins such as cigarette smoke induced senescent cell types using lung fibroblasts (Nyunoya et al., 2006) whereas high physical fitness has slowed the effects of ROS (Dai and Rabinovich, 2009). In opposition of the free radical theory of aging, publications have supported that increased mitochondrial ROS production actually mediates the detrimental effects seen after physical inactivity and that aging per se does not cause mitochondrial dysfunction (Gram et al., 2015). In conclusion, the data herein supports that through low levels of oxidative stress through exposure of hydrogen peroxide NIH/3T3 mouse embryonic fibroblasts mimics senesced characteristics such as enlarged and oval nuclear morphology, a decrease in mitotic proliferation, weakened mitochondrial and cellular membrane, and decreased levels of ROS and of ATP.

Future studies investigating the advantages and disadvantages of using H_2O_2 and possible ROS combinations to induce oxidative SIPS are concedable. Furthermore, it would also be interesting to see how mitochondrial function differs between neurons collected from mentally strong willed individuals versus the muscle fibers of physically strong individuals, as well as their opposites. Hydrogen peroxide alone is not enough to create a reliable model of aging, as many oxidative stressors and environmental factors are responsible of the varying rates of cellular aging in humans. As we continue to look for solutions of aging symptoms to ultimately halt death itself, the role of geriatric studies is steadily gaining ground on importance and recognition.

References

Abdollahi M, Moridani MY, Aruoma OI, and Mostafalou S. Editorial: Oxidative stress in aging. Oxidative Medicine and Cellular Longevity. 2014. doi: 10.1155/2014/876834

Alili L, Diekmann J, Giesen M, Holtkötter O, and Brenneisen P. A drug-induced accelerated senescence (DIAS) is a possibility to study aging in time lapse. Age (Dordr). 2014;36(3):9658. doi: 10.1007/s11357-014-9658-8

Apel K, Hirt H. Reactive oxygen species: Metabolism, oxidative Stress, and signal transduction. Annu. Rev. Plant Biol. 2004;55:373-399. doi: 10.1146/annurev.arplant.55.031903.141701

Atilano SR, Chwa M, Kim DW, Jordan N, Udar N, Coskun P, Jester JV, Wallace DC, Kenney MC. Hydrogen peroxide causes mitochondrial DNA damage in corneal epithelial cells. Cornea. 2009;28(4):426-433. doi: 10.1097/ICO.0b013e31818c2c55

Balaban RS, Nemoto S and Finkel T. Mitochondria, Oxidants, and Aging. Cell. 2005;120:483-495. doi: 10.1016/j.cell.2005.02.001

Bretón-Romero R, Lamas S. Hydrogen peroxide signaling in vascular endothelial cells. Redox Biology. 2014;2:529-534. doi: 10.1016/j.redox.2014.02.005

Brownlee M. Biochemistry and molecular cell biology of diabetic complications. Nature. 2001;414:813-820. doi: 10.1038/414813a

Bua E, Johnson J, Herbst A, Delong B, McKenzie D, Salamat S, and Aiken JM. Mitochondrial DNA–Deletion mutations accumulate intracellularly to detrimental levels in aged human skeletal muscle fibers. The American Journal of Human Genetics. 2006;79(3):469-480. doi: 10.1086/507132

Bürkle A, Moreno-Villanueva M, Bernhard J, Blasco M, Zondag G, Hoeijmakers JHJ, et al. MARK-AGE biomarkers of ageing. Mechanisms of Ageing and Development. 2015. doi: 10.1016/j.mad.2015.03.006

Chen C, Ames BN. Senescence-like growth arrest induced by hydrogen peroxide in human diploid fibroblast F65 cells. Proc. Natl. Acad. Sci. USA. 1994;91:4130–4134.

Cooper GM. (2000). The Cell: A Molecular Approach. 2nd edition. Sunderland (MA): Sinauer Associates.

Dai D, Chiao YA, Marcinek DJ, Szeto HH, and Rabinovitch PS. Mitochondrial oxidative stress in aging and healthspan. Longev Healthspan. 2014;3(4). doi: 10.1186/2046-2395-3-6

Dai D and Rabinovitch PS. Cardiac Aging in Mice and Humans: the Role of Mitochondrial Oxidative Stress. Trends Cardiovasc Med. 2009;19(7):213–220. doi: 10.1016/j.tcm.2009.12.004

de Oliveira-Marques V, Cyme L, Marinho HS, Antunes F. A Quantitative Study of NF-κB Activation by H2O2: Relevance in Inflammation and Synergy with TNF-α. The Journal of Immunology. 2007;178(6):3893-3902. doi: 10.4049/ jimmunol.178.6.3893

Dimri GP, Itahana K, Acosta M, Campisi J. Regulation of a senescence checkpoint response by the E2F1 transcription factor and p14/ARF tumor suppressor. Mol Cell Biol. 2000;20:273–285.

Dröge W and Schipper HM. Oxidative stress and aberrant signaling in aging and cognitive decline. Aging Cell. 2007;6(3):361-370. doi: 10.1111/j.1474-9726.2007.00294.x

Duan Jianming, Duan Jianping, Zhang Z, Tong, T. Irreversible cellular senescence induced by prolonged exposure to H_2O_2 involves DNA-damage-and-repair genes and telomere shortening. Int J Biochem & Cell Bio. 2005;37:1407-1420. doi: 10.1016/j.biocel.2005.01.010

Fernandez-Guerra P, Lund M, Corydon TJ, Cornelius N, Gregersen N, Palmfeldt J, et al. Application of an image cytometry protocol for cellular and mitochondrial phenotyping on fibroblasts from patients with inherited disorders. JIMD Reports. 2015. doi: 10.1007/8904_2015_494

Gram M, Vigelsø A, Yokota T, Helge JW, Dela F, Hey-Mogensen M. Skeletal muscle mitochondrial H_2O_2 emission increases with immobilization and decreases after aerobic training in young and older men. J Physiol. 2015;593(17):4011-4027. doi: 10.1113/JP270211

Halliwell B, Clement MV, Long LH. Hydrogen peroxide in the human body. FEBS Letters. 2000;486(1):10-13. doi: 10.1016/S0014-5793(00)02197-9

Han H, Long H, Wang H, Wang J, Zhang Y. Progressive apoptotic cell death triggered by transient oxidative insult in H9c2 rat ventricular cells: a novel pattern of apoptosis and the mechanisms. Am J Physiol Heart Circ Physiol. 2004;286:H2169–H2182. doi: 10.1152/ajpheart.00199.2003

Harman D. Aging: a theory based on free radical and radiation chemistry. J Gerontol. 1956 Jul;11(3):298-300.

Herbst A, Pak JW, McKenzie D, Bua E, Bassiouni M, and Aiken JM. Accumulation of Mitochondrial DNA deletion mutations in aged muscle fibers: Evidence for a causal role in muscle fiber loss. J Gerontol A Biol Sci Med Sci. 2007;62(3):235-245.

Holbrook NJ, Finkel, T. Oxidants, oxidative stress and the biology of ageing. Nature. 2000;408:239-247. doi:10.1038/35041687

Kokoszka JE, Coskun P, Esposito LA, and Wallace DC. Increased mitochondrial oxidative stress in the Sod2 (+/-) mouse results in the age-related decline of mitochondrial function culminating in increased apoptosis. PNAS. 2001;98(5):2278-2283. doi: 10.1073/pnas.051627098

Kujoth GC, Bradshaw PC, Haroon S, Prolla TA. The role of mitochondrial DNA mutations in mammalian aging. PLoS Genet. 2007;3(2):161-173. doi:10. 1371/journal.pgen.0030024

Lanza IR and Sreekumaran Nair K. Muscle mitochondrial changes with aging and exercise. Am J Clin Nutr. 2009;89(1):467S-471S. doi: 10.3945/ajcn.2008.26717D

Li M, Zhao L, Liu J, Liu A, Zeng W, Luo S, Bai X. Hydrogen peroxide induces G2 cell cycle arrest and inhibits cell proliferation in osteoblasts. The Anatomical Record. 2009;292:1107-1113. doi: 10.1002/ar.20925

Liochev S. Reactive oxygen species and the free radical theory of aging. Free Radical Biology and Medicine. 2013;60:1-4. doi:10.1016/j.freeradbiomed.2013.02.011

Liu T, Hannafon B, Gill L, Kelly W, and Benbrook D. Flex-Hets differentially induce apoptosis in cancer over normal cells by directly targeting mitochondria. Mol Cancer Ther. 2007;6:1814-1822. doi:10.1158/1535-7163.MCT-06-0279

Lodish H, Berk A, Zipursky SL, et al. (2000). Molecular Cell Biology. 4th edition. New York: W. H. Freeman.

Lopez ME, Van Zeeland NL, Dahl DB, et al. Cellular phenotypes of age-associated skeletal muscle mitochondrial abnormalities in rhesus monkeys. Mutat Res. 2000;452(1): 123-138.
López-Otín C, Blasco MA, Partridge L, Serrano M, Kroemer G. The hallmarks of aging. Cell. 2013;153:1194-1217. doi: 10.1016/j.cell.2013.05.039
Maechler P and Wollheim CB. Mitochondrial function in normal and diabetic ß-cells. Nature. 2001;414:807-812. doi: 10.1038/414809
McConnell BB, Starborg M, Brookes S, Peters G. Inhibitors of cyclin- dependent kinases induce features of replicative senescence in early passage human diploid fibroblasts. Curr Biol. 1998;8:351–354.
Navarro A, Gomez C, López-Cepero JM, Boveris A. Beneficial effects of moderate exercise on mice aging: survival, behavior, oxidative stress, and mitochondrial electron transfer. Am J Physio (RICP). 2004;286(3):R505-R511. doi: 10.1152/ajpregu.00208.2003
Orrenius S, Gogvadze V, and Zhivotovsky. Mitochondrial oxidative stress: Implications for cell death. Annual Review of Pharmacology and toxicology. 2007;47:143-183. doi: 10.1146/annurev.pharmtox.47.120505.105122
Pendergrass W, Wolf N, and Poot M. Efficacy of MitoTracker Green™ and CMXrosamine to measure changes in mitochondrial membrane potentials in living cells and tissues. Cytometry. 2004;61A:162-169. doi: 10.1002/cyto.a.20033
Serra V, von Zglinicki T, Lorenz M, Saretzki G. Extracellular superoxide dismutase is a major antioxidant in human fibroblasts and slows telomere shortening. J. Biol. Chem. 2003;278:6824–6830.
Simm A, Nass N, Bartling B, Hofmann B, Silber R and Santos AN. Potential biomarkers of ageing. Biol Chem. 2008;389:257-265. doi: 10.1515/BC.2008.034
Someya S, Xu J, Kondo K, Ding D, Salvi RJ, Yamasoba T, Rabinovitch PS, Weindruch R, Leeuwenburgh C, Tanokura M, Prolla TA. Age-related hearing loss in C57BL/6 J mice is mediated by Bak-dependent mitochondrial apoptosis. Proc Natl Acad Sci U S A. 2009;106:19432–19437. doi: 10.1073/pnas.0908786106
Sood S, Gallagher IJ, Lunnon K, Rullman E, Keohane A, Crossland H, et al. A novel multi-tissue RNA diagnostic of healthy ageing relates to cognitive health status. Genome Biology. 2015;16:185. doi: 10.1186/s13059-015-0750-x
Roberg K, Johansson U, Öllinger K. Lysosomal release of Cathepsin D precedes relocation of Cytochrome C and loss of mitochondrial transmembrane potential during apoptosis induced by oxidative stress. Free Radical Biology and Medicine. 1999;27(11-12):1228-1237. doi:10.1016/S0891-5849(99)00146-X
Taanman J. The mitochondrial genome: structure, transcription, translation and replication. Biochimica et Biophysica Acta. 1999;1410:103-123. doi:10.1016/S0005-2728(98)00161-3
Taylor RW and Turnbull DM. Mitochondrial DNA mutations in human disease. Nat Rev Genet. 2005;6:389-402. doi: 10.1038/nrg1606
Trifunovic A, Wredenberg A, Falkenberg M, Spelbrink JN, Rovio AT, Bruder CE, Bohlooly-Y M, Gidlöf S, Oldfors A, Wibom R, Törnell J, Jacobs HT, Larsson NG. Premature ageing in mice expressing defective mitochondrial DNA polymerase. Nature. 2004;429(6990):417-23.

Trifunovic A. Mitochondrial DNA and ageing. Biochimica et Biophysica Acta. 2006;1757(5-6):611-617. doi: 10.1016/j.bbabio.2006.03.003

Van Raamsdonk JM, Hekimi S. Superoxide dismutase is dispensable for normal animal lifespan. Proc. Natl. Acad. Sci. USA, 2012;109:5785–5790.

Vock R, Hoppeler H, Claassen H, Wu DXY, Billeter R, Weber J, Taylor CR, and Weibel ER. Design of the oxygen and substrate pathways: VI. Structural basis of intracellular substrate supply to mitochondria in muscle cells. The Journal of Experimental Biology. 1996;199:1689–1697

Appendix A

Table A1. Cytotoxicity and morphology of H_2O_2 treated NIH/3T3 raw data. NIH/3T3 reaching 70%-80% confluence was treated with varying concentrations of H_2O_2 at 37ºC (2 h). Cells were observed post-incubation over a period of 72 h. By randomization, 25 cells per 10 regions were counted for a normalized count of 250 total cells at t=0, 24, 48 h.

Time after H_2O_2 treatments (h)	Concentration (µM)	Normal	Autophagic	Necrotic	Apoptotic	Total Counted Cells
t=0	0	164	71	13	2	250
	5	156	65	23	6	250
	15	4	16	7	3	30*
	30	20	134	67	29	250
	50	105	88	33	24	250
	100	115	72	24	39	250
	200	23	147	34	46	250
	300	21	80	84	65	250
t=24	0	176	53	8	13	250
	5	94	107	34	15	250
	15	144	53	15	38	250
	30	103	80	48	19	250
	50	78	87	66	19	250
	100	131	68	27	24	250
	200	12	90	69	79	250

	300	**20**	**68**	**83**	**79**	**250**
t=48	**0**	**148**	**73**	**10**	**19**	**250**
	5	**100**	**97**	**46**	**7**	**250**
	15	**94**	**114**	**29**	**13**	**250**
	30	**109**	**101**	**31**	**9**	**250**
	50	**94**	**98**	**32**	**26**	**250**
	100	**130**	**65**	**31**	**24**	**250**
	200	**21**	**79**	**99**	**51**	**250**
	300	**6**	**71**	**90**	**83**	**250**
Note. ***Poor growth prior to treatment making it unable to count post-treatment.**						

Appendix B

Table B1. Raw JC-1 and MitoTracker CMXRos Data.
Post-H_2O_2 treated NIH/3T3 mouse embryonic fibroblast cells were incubated with 10 µg/ml JC-1 dye for 15 min and 50 µM CMXRos dye for 30 min at 37ºC. Relative luminescence (RT) of cells were measured at excitation wavelengths of ≥ 488 nm and ≥ 580 nm using the PerkinElmer 2030 Multilabel Reader Victor™ X2.

Trial	H_2O_2 Concentrations (µM)	Control		Treated Control		JC-1 Dyed Treated		CMXRos Dyed Treated
		RL at 488 nm	RL at 580 nm	RL at 488 nm	RL at 580 nm	RL at 488 nm	RL at 580 nm	RL at 580 nm
A	0	442352	209921	632394	168589	186566	995226	57948
	50	699256	297449	509093	963411	462867	998036	297117
	200	442322	240104	698803	925554	106531	628919	771375
	300	582089	537252	198047	342588	103449	443349	209951
B	0	631790	608102	250437	197050	912441	618556	85835
	50	457096	471689	608677	701522	730406	52782	821801
	200	601848	638376	588766	357785	671097	976765	453773
	300	856245	830503	499516	89581	321861	573508	305758
C	0	628527	723699	743337	615928	312767	182185	506193
	50	570094	381382	624176	694210	117468	870354	329808
	200	192428	740527	806483	157622	852710	746872	320744
	300	559580	906036	580276	869055	163332	333645	959483

Table B2. Averaged JC-1 and MitoTracker CMXRos Data.
Averaged data obtained using raw data supplied by three independent trials.

Trial	H_2O_2 Concentrations (µM)	Control		Treated Control		JC-1 Dyed Treated		CMXRos Dyed Treated
		RL at 488 nm	RL at 580 nm	RL at 488 nm	RL at 580 nm	RL at 488 nm	RL at 580 nm	RL at 580 nm
A	0	541505	321182	632394	168589	186566	995226	57948
	50			509093	963411	462867	998036	297117
	200			698803	925554	106531	628919	771375
	300			198047	342588	103449	443349	209951
B	0	636745	637168	250437	197050	912441	618556	85835
	50			608677	701522	730406	52782	821801
	200			588766	357785	671097	976765	453773
	300			499516	89581	321861	573508	305758
C	0	487657	687911	743337	615928	312767	182185	506193

	50			624176	694210	117468	870354	329808
	200			806483	157622	852710	746872	320744
	300			580276	869055	163332	333645	959483
All	0	1665907	1646260	1626168	981567	1411774	1795967	649976
	50			1741946	2359143	1310741	1921172	1448726
	200			2094052	1440961	1630338	2352556	1545892
	300			1277839	1301224	588642	1350502	1475192

Table B3. Normalized JC-1 and MitoTracker Data.

H_2O_2 Concentrations (µM)	**JC-1 Ratio Raw**	**JC-1 Ratio Normalized**	**MitoTracker Raw**	**MitoTracker Normalized**
0	-3.798613767	0	-331591	0
50	1.015690913	4.81430468	-910417	-578826
200	-1.96585611	1.832757658	104931	436522
300	-0.071500601	3.727113166	173968	505559

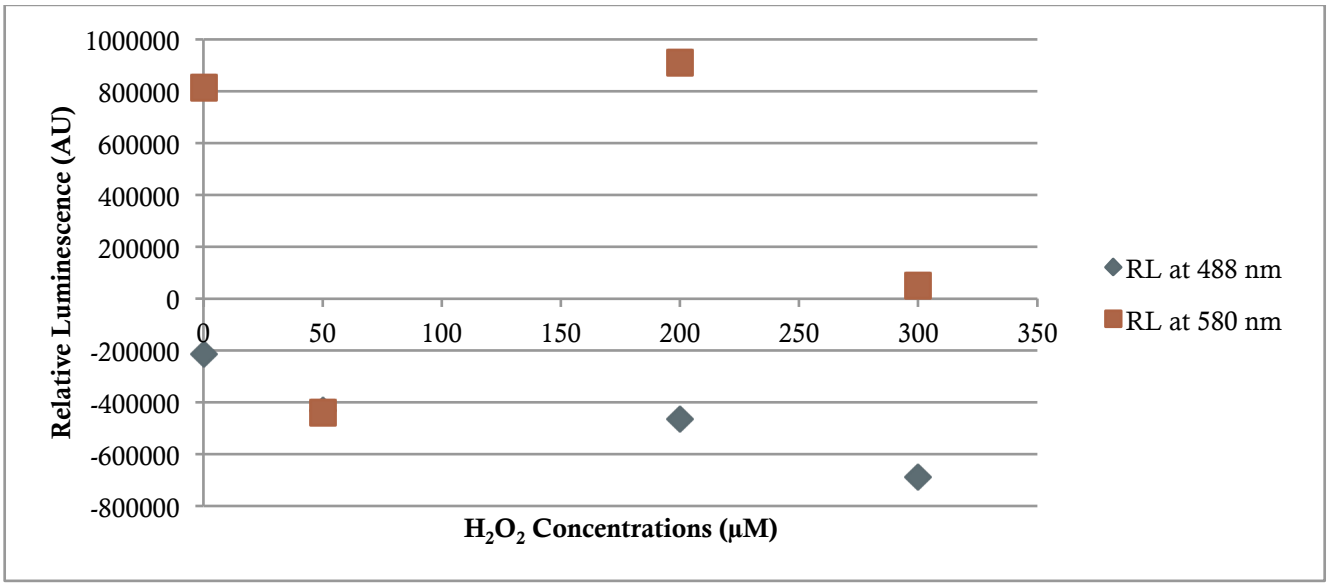

Figure B1. JC-1 ratio raw of RL at ≥ 488 nm versus ≥ 580 nm.

Appendix C

Table C1. Raw ROS levels after H_2O_2 Treatments.
Using the ROS-Glo™ H_2O_2 Assay (Promega) according to the manufacturer's instructions control and treated H_2O_2 cells were used to measure H_2O_2 levels.

ROS Levels after H_2O_2 Treatments								
Trial	H_2O_2 Concentrations (µM)	Relative Luminescence (AU)						
		Value 1	Value 2	Value 3	Value 4	Value 5	Value 6	Average
A	0	367514	858088	236207	864946	237143	257054	470159
	50	546981	984983	63266	90609	529427	432533	441300
	200	103721	266208	892621	240437	155084	133844	298653
	300	932322	89309	56619	68130	343041	915553	400829
B	0	438455	946703	838811	538884	843676	696597	717188
	50	403709	266571	14290	530333	955254	404706	429144
	200	248685	589703	262583	687171	945827	441144	529186
	300	891322	17100	941567	605534	788295	580910	637455
C	0	230104	389177	14229	423741	91424	663332	302001
	50	856547	74203	812949	665447	694573	804670	651398
	200	534835	688772	151337	692609	730617	779956	596354
	300	40757	869992	648075	709498	94597	556468	486565
All	0							1489348
	50							1521842
	200							1424192
	300							1524848

Table C2. Normalized ROS data.

Raw ROS	Normalized ROS
1489348	65155
1521842	97649
1424192	0
1524848	100656

Table C3. ROS standard.

ROS Standard (µM)	Relative Luminescence (AU)			
	Value 1	Value 2	Value 3	Average
0	443047	612725	224061	426611

100	339627	85684	565109	330140
200	503564	312254	257567	357795
300	48612	89249	729862	289241
400	384433	876034	867937	709468
500	240708	311226	238775	263570
600	937972	783702	198803	640159
700	860928	933560	452323	748937
800	702640	588131	286512	525761
900	606320	412955	875672	631649
1000	564021	503595	308386	458667

Appendix D

Table D1. Raw ATP levels after H_2O_2 Treatments.
Using the ENLITEN® ATP Assay System Bioluminescence Detection Kit (Promega) levels of ATP were measured according to the manufacturer's instructions.

Trial	H_2O_2 Concentrations (µM)	Relative Luminescence (AU)						
		Value 1	Value 2	Value 3	Value 4	Value 5	Value 6	Average
A	0	596289	207595	949966	877243	397788	987582	669411
	50	193455	896761	578705	447640	631065	711432	576510
	200	59126	292706	267598	413559	896368	713094	440409
	300	731161	897093	399631	403437	904828	315517	608611
B	0	574868	360021	736358	747900	739017	742038	650034
	50	147923	208169	279865	683636	912018	374161	434295
	200	522478	118284	908362	211039	522780	658287	490205
	300	444135	690766	99522	88766	85019	37524	240955
C	0	314157	700314	151247	400899	77164	678983	387127
	50	727687	206718	697081	619553	658347	548552	576323
	200	107317	549912	59126	974832	469393	970270	521808
	300	730587	535651	683122	695872	378391	394736	569727
All	0							1706572
	50							1587128
	200							1452422
	300							1419293

Table D2. Normalized ATP data.

Raw ATP	Normalized ATP
1706572	0
1587128	-119444
1452422	-254150
1419293	-287279

Table D3. ATP standard.

ATP Standard (nmol)	Relative Luminescence (AU)			
	Value 1	Value 2	Value 3	Average
0	742068	903105	969393	871522
2	144419	467641	505438	372499
4	521360	770227	709317	666968
6	29880	60003	273278	121054

8	16918	634660	824128	491902
10	750830	33928	650159	478306